HRI-RECAPP-2015-014

Reduced LHC constraints for higgsino-like heavier electroweakinos

Manimala Chakraborti[a1], Utpal Chattopadhyay[a2], Arghya Choudhury[b3], Amitava Datta[c4] and Sujoy Poddar[d5]

[a] Department of Theoretical Physics, Indian Association for the Cultivation of Science, 2A & B Raja S.C. Mullick Road, Jadavpur, Kolkata 700 032, India

[b] Regional Centre for Accelerator-based Particle Physics, Harish-Chandra Research Institute, Allahabad 211019, India

[c] Department of Physics, University of Calcutta, 92 A.P.C. Road, Kolkata 700 009, India

[d] Department of Physics, Netaji Nagar Day College, Kolkata 700092, India

arXiv:1507.01395v2 [hep-ph] 18 Nov 2015

Abstract

As a sequel to our earlier work on wino-dominated $\tilde{\chi}_1^\pm$ and $\tilde{\chi}_2^0$ (wino models), we focus on the pMSSM models where $\tilde{\chi}_1^\pm$, $\tilde{\chi}_2^0$ and $\tilde{\chi}_3^0$ are either higgsino dominated (higgsino models) or admixtures of significant amount of higgsino and wino components (mixed models), with or without light sleptons. The LHC constraints in the trilepton channel are significantly weaker even in the presence of light sleptons, especially in the higgsino models, compared to those mostly studied by the LHC collaborations with wino-dominated $\tilde{\chi}_1^\pm$ and $\tilde{\chi}_2^0$. The modes $\tilde{\chi}_3^0, \tilde{\chi}_2^0 \to \tilde{\chi}_1^0\, h$ with large branching ratios (BRs) are more common in the higgsino models and may produce spectacular signal in the LHC Run-II. In a variety of higgsino and mixed models we have delineated the allowed parameter space due to the LHC constraints, the observed Dark Matter (DM) relic density of the universe, which gets contributions from many novel DM producing mechanisms i.e., the annihilation/coannihilation processes that lead to the correct range of relic density, and the precise measurement of the anomalous magnetic moment of the muon. In the higgsino models many new DM producing mechanisms, which are not allowed in the wino models, open up. We have also explored the prospects of direct and indirect detection of DM in the context of the LUX and IceCube experiments respectively. In an extended model having only light gluinos in addition to the electroweak sparticles, the gluinos decay into final states with multiple taggable b-jets with very large BRs. As a consequence, the existing ATLAS data in the $0l$ + jets (3b) + $\not{E}_T$ channel provide the best limit on $m_{\tilde{g}}$ ($\approx$ 1.3 TeV). Several novel signatures of higgsino models for LHC Run-II and ILC have been identified.

[1]tpmc@iacs.res.in, [2]tpuc@iacs.res.in, [3]arghyachoudhury@hri.res.in, [4]adatta@iiserkol.ac.in,

[5]sujoy.phy@gmail.com

Contents

1 Introduction **3**

2 Production of chargino-neutralino pairs in different models **8**

3 The Methodology **10**

3.1 The Constraints 10

3.2 The Simulation 12

3.3 Scanning the parameter space 12

4 The $\widetilde{\chi}_1^{\pm}$-Higgsino and $\widetilde{\chi}_1^{\pm}$-Mixed Models with Light Left and Right Sleptons **13**

4.1 A brief review of the Light Wino and light Left and Right Sleptons (LWLRS) model 13

4.2 The Light Higgsino and light Left and Right Sleptons (LHLRS) model 15

4.3 The Light Mixed $\widetilde{\chi}_1^{\pm}$ with light Left and Right Sleptons (LMLRS) model 20

5 The Higgsino and Mixed Models with Light Left Sleptons **23**

5.1 A brief review of the Light Wino and light Left Sleptons (LWLS) model 23

5.2 The Light Higgsino and light Left Sleptons (LHLS) model 24

5.3 The Light Mixed $\widetilde{\chi}_1^{\pm}$ and light Left Sleptons (LMLS) model 25

6 The Light Higgsino and Heavy Sleptons (LHHS) model **27**

7 Direct Detection via Spin-independent scattering **27**

7.1 LHLRS and LMLRS 28

7.2 LHLS and LMLS 30

7.3 LHHS 30

8 Spin-dependent (SD) direct detection cross-section and indirect detection reach for muon flux **31**

8.1 LHLRS and LMLRS 33

8.2 LHLS and LMLS 35

8.3 LHHS 35

9 New constraints on $m_{\widetilde{g}}$ and future search prospects **37**

10 Conclusion **43**

1 Introduction

The first phase of the p-p collision at the Large Hadron Collider (LHC) (Run-I) has given lower limits on the masses of the super-particles (sparticles) for models involving supersymmetry [1–3], although the latter is yet to be discovered. The bounds on the masses of the strongly interacting sparticles are already stringent [4–9][1]. Searches have just been started at the new round of experiments at higher energies (13 TeV). However, the possibility that these sparticles are even beyond the reach of the ongoing experiments as well is wide open. It is known that this scenario is indeed favoured by the SUSY flavour and SUSY CP problems [2]. On the other hand, we also note that heavy squarks belonging to the first two generations do not spoil the naturalness [11, 12] of a SUSY model.

It is remarkable that the observed mass of the Higgs boson at around 125 GeV [13] at CERN is well within the MSSM predicted upper limit of M_h ($\lesssim$ 135 GeV), where M_h refers to the mass of the CP even neutral lighter Higgs boson h. In this analysis we consider the decoupled Higgs scenario of the MSSM, namely $M_A >> M_Z, M_h$ [2, 3], where M_A refers to the mass of the pseudoscalar Higgs boson. In the decoupling limit h becomes Standard Model like in its couplings [14]. It is well known that the current Higgs data are indeed consistent with the decoupling limit [15].

If the heavy squark-gluino scenario along with a decoupled Higgs sector is indeed realized in nature, we must accept that the observability of SUSY signals hinges on the properties of the sparticles in the electroweak (EW) sector[2]. Although the production cross-sections of these sparticles are rather modest, significant bounds on their masses have already been obtained by both the ATLAS and CMS collaborations of the LHC [16–21] from the null results of (i) chargino ($\widetilde{\chi}_1^{\pm}$) - neutralino ($\widetilde{\chi}_2^0$) searches[3] via the process $pp \to \widetilde{\chi}_1^{\pm}\widetilde{\chi}_2^0$ leading to the trilepton + transverse missing energy ($\not{E}_T$) signal and (ii) slepton searches via the opposite sign same flavour dilepton

[1] However in compressed SUSY type scenarios limits on sparticle masses are considerably weaker [10].

[2] The fermionic members of this sector, the charginos and the neutralinos, are referred to as the electroweakinos while the scalar members are sleptons of both L and R types and sneutrinos.

[3] Throughout this paper chargino would stand for the lighter chargino ($\widetilde{\chi}_1^{\pm}$) unless otherwise mentioned and the four neutralinos $\widetilde{\chi}_1^0 - \widetilde{\chi}_4^0$ are arranged in order of ascending masses.

+ $\not{E}_T$ channel. We shall focus on the analyses performed by the ATLAS group. They obtained model independent upper bounds on the cross-sections of these processes applicable to any Beyond the Standard Model (BSM) scenario corresponding to different signal regions each characterized by an appropriate set of selection criteria. The results were interpreted in terms of several simplified models. A large number of phenomenological analyses have addressed the electroweakino searches and related topics in the context of the LHC [22–24].

The discovery potentials of the charginos and the neutralinos depend on their pair production cross-sections and decay branching ratios (BRs) into leptonic channels which contribute to the trilepton signal[4]. These observables depend - among other things - on their compositions. The focus of this paper is on the phenomenology of models where $\widetilde{\chi}_1^{\pm}$, $\widetilde{\chi}_2^0$ and $\widetilde{\chi}_3^0$ are either higgsino dominated or admixtures of significant amount of higgsino and wino components. In the following, we shall refer to :

i) the former class of models as the $\widetilde{\chi}_1^{\pm}$-*higgsino* or simply, the *higgsino models*, and

ii) the latter class of models as $\widetilde{\chi}_1^{\pm}$-*mixed* or simply, the *mixed models*.

On the other hand, the LHC collaborations restricted their analyses of chargino-neutralino search in the trilepton channel to simplified scenarios where the lighter chargino ($\widetilde{\chi}_1^{\pm}$) and the second lightest neutralino ($\widetilde{\chi}_2^0$) are wino dominated and are nearly mass degenerate. All models belonging to this class will be referred to as the $\widetilde{\chi}_1^{\pm}$-*wino* or simply, the *wino models*. As in the analyses of the ATLAS or the CMS collaborations the lightest supersymmetric particle (LSP), i.e., the lightest neutralino ($\widetilde{\chi}_1^0$) is considered to be strongly bino-dominated over the parameter space with $m_{\widetilde{\chi}_1^{\pm}} >> m_{\widetilde{\chi}_1^0}$. In the *higgsino models* this is ensured by the chosen hierarchy $\mu = M_2/2 >> M_1$, where M_1, M_2 and μ are the U(1), SU(2) gaugino and higgsino mass parameters respectively. In some regions where μ satisfies $\mu = M_2/2 \gtrsim M_1$ the LSP gets non-negligible higgsino components.

In the backdrop of the basic varieties for the compositions of the electroweakinos and the correlation of slepton masses with that of the electroweakinos, that we are going to enumerate shortly, one of the main goals of this paper is to go beyond the *wino* models and reinterpret the ATLAS data in several *higgsino* and *mixed models*. Before we move on to the above models, we would like to set the background briefly by digging into the analysis of the $\widetilde{\chi}_1^{\pm}$- *wino* scenario.

[4]In this work lepton usually implies electrons and muons unless mentioned otherwise.

$\widetilde{\chi}_1^{\pm}$- *wino*: Each simplified *wino model* considered by ATLAS and CMS analyses [16, 19–21] belongs to either of the two following broad categories. In one case, sleptons of all three flavours are heavier than the winos (the **L**ight **W**ino and **H**eavy **S**lepton model (LWHS))[5]. In the other category, at least one type of slepton of all flavours (i.e., either L or R-type or both) is lighter than $\widetilde{\chi}_1^{\pm}$ and $\widetilde{\chi}_2^0$. The BRs of the electroweakinos and consequently, the discovery channels in the two scenarios may be significantly different. The second category in turn consists of several subcategories depending on the type of the light sleptons, and their masses with respect to $m_{\widetilde{\chi}_1^0}$ and $m_{\widetilde{\chi}_1^{\pm}}$, some of which were considered by the ATLAS group while the CMS collaboration as well as the analysis of Ref. [24] studied more variations. The important features of each subcategory will be summarized in the latter sections. In the *wino models* $\widetilde{\chi}_1^{\pm}$ and $\widetilde{\chi}_2^0$ production followed by their decays into trileptons is the main discovery channel in most cases.

We wish to stress that in Ref. [24] as well as in this work we do not restrict ourselves to stay within the decoupled slepton scenario. The presence of relatively light sleptons has two important implications. First, the constraints from the direct slepton searches at the LHC must be included in our analysis. Moreover, the possibility that the sleptons play active roles in DM production[6] is resurrected, as has already been noted in Ref. [24] and will be further illustrated in this analysis.

The slepton search results, mainly for the selectron ($\widetilde{e}$) and the smuon ($\widetilde{\mu}$) are fairly insensitive to the electroweakino sector. We particularly note that sleptons of the first two generations have negligible L-R mixing, which in turn means that there is hardly any dependence of μ or $\tan\beta$ in determining the masses of these sleptons or their couplings with the gauge bosons. Any slepton lighter than $\widetilde{\chi}_1^{\pm}$ or $\widetilde{\chi}_2^0$ decays into its fermionic superpartner and $\widetilde{\chi}_1^0$ with 100% BR and this is independent of the composition of $\widetilde{\chi}_1^{\pm}/\widetilde{\chi}_1^0$. Subject to these general assumptions mass bounds were obtained by the LHC collaborations in several simplified models [17, 21]. In view of the above independence we shall directly use the constraints from the slepton searches as derived in Ref. [24] for the *wino models*.

[5] In Reference [24] this model was called the **L**ight **G**augino and **H**eavy **S**lepton (LGHS) model but we find the terminology LWHS to be better suited for discriminating between the *wino* and the *higgsino models*. A similar change in nomenclature applies to all the models discussed in Ref. [24].

[6] *The DM producing mechanism* which would often be quoted in this work would mean annihilation/coannihilation processes that bring the DM relic density within the acceptable range given by the WMAP/PLANCK data.

The models studied by the ATLAS collaboration[7] to interpret their search results are in some sense oversimplified. The parameters of such a model provide a minimal set to understand important aspects of a SUSY signal. However, in order to test SUSY in the light of the LHC as well as other constraints from the so called indirect tests, one requires a closely related but a complete model like the phenomenological minimal supersymmetric standard model (pMSSM) [25] with additional parameters. In Ref. [24] we enlarged each simplified *wino model* by introducing a minimal set of parameters belonging to the EW sector (like μ and $\tan\beta$) and tried to scrutinize the pMSSM thus obtained by considering three major constraints, namely, the LHC mass limits on the chargino-neutralino and the slepton sectors, measured dark matter (DM) [26–28] relic density of the universe from the WMAP [29]/PLANCK [30][8] and the precisely measured value of $(g-2)_\mu$ [35]. Moreover, we dispensed with the unrealistic assumption $m_{\widetilde{\nu}} = m_{\widetilde{\ell}_L}$ which leads to erroneous LHC limits especially if $m_{\widetilde{\chi}_2^0} \approx m_{\widetilde{\ell}_L}$. These modifications change the LHC limits quite significantly in some models and we computed these changes in Ref. [24] by a PYTHIA (v6.428) [36] based analysis using ATLAS data. New bounds for several wino-slepton mass hierarchies not considered by the ATLAS collaboration were also derived. For each model, compatibility with the three major constraints delineates an allowed parameter space (APS). Each APS, in turn, enables us to focus on the expected SUSY signals in the future LHC experiments.

$\widetilde{\chi}_1^\pm$- higgsino or mixed: In this paper we extend our earlier analysis to the $\widetilde{\chi}_1^\pm$-*higgsino* and $\widetilde{\chi}_1^\pm$-*mixed models*. The mass hierarchies among the sleptons and electroweakinos are, however, similar to the ones in [24]. In Table 1 we present the models analyzed in this paper and the choice of parameters for each of them. In our analysis, M_1 and M_2 are free parameters.

As mentioned earlier the LSP is also assumed to be bino-dominated with some degree of higgsino mixing, depending on the parameter space. Finally, we delineate the APSs in both the models while isolating the effects of each major constraint clearly. We emphasize that in the post-LHC era, these models, especially the *higgsino models*, have not received due attention in the literature. Yet, the difference in phenomenology of the *higgsino models* and that of the *wino models* is indeed worth noting. Firstly, the LHC exclusion contours from the trilepton searches shrink significantly in the *higgsino models* and even become irrelevant in some scenarios. As we will see later the physics of

[7] Similar simplified models were also analysed by the CMS collaboration.

[8] A partial list of works on SUSY DM may be seen in Ref. [31–34].

	Model	Acronym	Parameter Choice
$\widetilde{\chi}_1^{\pm}$-Higgsino	Light Higgsino and light Left and Right Sleptons	LHLRS (Sec.4.2)	$\mu = \frac{M_2}{2}$ $m_{\widetilde{l}_L} = m_{\widetilde{l}_R} = (m_{\widetilde{\chi}_1^0} + m_{\widetilde{\chi}_1^{\pm}})/2$
	Light Higgsino and light Left Sleptons	LHLS (Sec.5.2)	$\mu = \frac{M_2}{2}$ $m_{\widetilde{l}_L} = (m_{\widetilde{\chi}_1^0} + m_{\widetilde{\chi}_1^{\pm}})/2, m_{\widetilde{l}_R} = 2$ TeV
	Light Higgsino and Heavy Sleptons	LHHS (Sec.6)	$\mu = \frac{M_2}{2}$ $m_{\widetilde{l}_{L,R}} = \mu + 200$ GeV
$\widetilde{\chi}_1^{\pm}$-Mixed	Light Mixed and light Left and Right Sleptons	LMLRS (Sec.4.3)	$\mu = 1.05 M_2$ $m_{\widetilde{l}_L} = m_{\widetilde{l}_R} = (m_{\widetilde{\chi}_1^0} + m_{\widetilde{\chi}_1^{\pm}})/2$
	Light Mixed and light Left Sleptons	LMLS (Sec.5.3)	$\mu = 1.05 M_2$ $m_{\widetilde{l}_L} = (m_{\widetilde{\chi}_1^0} + m_{\widetilde{\chi}_1^{\pm}})/2, m_{\widetilde{l}_R} = 2$ TeV

Table 1: Summaries of the models analyzed in this work. The parameter choice for each case is presented in the last column. For all the analyses we take $M_1 << M_2$, $M_1 \lesssim \mu$ to make the LSP predominantly a bino. Two representative values of $\tan\beta = 6$ and 30 are considered in this analysis. For the LHHS model, however, we consider only $\tan\beta = 30$ case for reasons discussed in the text.

DM relic density and $(g-2)_\mu$ in the *higgsino models* are also quite distinctive. All these points will be elaborated in the rest of this paper.

We will further confront each APS thus obtained with other constraints like those from direct [37, 38] and indirect [39, 40] dark matter searches. We include current limits as well as compare our results in relation to future reaches of these experiments [39, 41]. We also keep in mind the sizable uncertainties involved in these constraints (see Ref. [24] and the references therein). We emphasize that unlike the analysis of Ref. [24], here we have a sizable amount of higgsino content within the LSP because μ and M_1 are not widely separated. This leads to a considerable increase in the spin-independent LSP-nucleon scattering cross-section. Additionally, a larger higgsino content within the LSP generically increases the spin-dependent LSP-nucleon cross-section. This, in turn, increases the gravitational capture cross-section of the LSPs within astrophysically dense regions like the core of the Sun. In addition, the LSPs with larger higgsino content may potentially contribute to neutrinos created within the Sun via LSP pair annihilation. Thus, the IceCube experiment puts

limits on the muon flux at the detector site which are not far away from the predictions of the models.

We next consider an extended scenario in which only one strongly interacting sparticle is within the reach of the LHC-13/14 TeV experiments and assume this sparticle to be the gluino. The purpose is to study the feasibility of characterizing different *higgsino models* from their gluino decay signatures. We explore the gluino mass limits obtained at the LHC-8 TeV experiments via the n-leptons + m-jets (with or without b-tagging) + $\not{E}_T$ signals with different values of m and n [4–7]. By selecting a few benchmark points (BPs) with different characteristics we compute the revised gluino mass limits at the generator level by using PYTHIA (v6.428) [36]. This gives the sensitivity of various *higgsino models* to signals with different values of m and n and helps to anticipate the future search prospects.

The plan of the paper is as follows. We note that because of the enhancement of higgsino components within $\widetilde{\chi}_2^0$, $\widetilde{\chi}_3^0$ and $\widetilde{\chi}_1^\pm$, the production cross-sections of $\widetilde{\chi}_1^\pm$-$\widetilde{\chi}_2^0$ and $\widetilde{\chi}_1^\pm$-$\widetilde{\chi}_3^0$ in the $\widetilde{\chi}_1^\pm$-*higgsino* ($\widetilde{\chi}_1^\pm$-*mixed) models* are significantly (modestly) reduced from those in the $\widetilde{\chi}_1^\pm$-*wino models*. The characteristics of various cross-sections will be discussed in Sec. 2 with numerical examples. The relevant constraints for the *higgsino* and *mixed* models as well as the procedures for parameter space scanning and simulation of the trilepton signal will be discussed in Sec.3. The parameter spaces allowed by the main constraints in the $\widetilde{\chi}_1^\pm$-*higgsino* and $\widetilde{\chi}_1^\pm$-*mixed models* characterized by different mass hierarchies among the sleptons and the elctroweakinos will be presented in Secs. 4-6. We will explore the prospects of direct and indirect detection of dark matter in Sec. 7 and Sec. 8 respectively. The extended models with a light gluino and electroweak sparticles, introduced in the last paragraph, will be taken up in Sec. 9. Our main results and the conclusions are summarized in Sec. 10.

2 Production of chargino-neutralino pairs in different models

The size of the chargino - neutralino production cross-section with different neutralinos accompanying $\widetilde{\chi}_1^\pm$ is significantly different in the *wino*, *higgsino* and *mixed models*. In the *wino models* the main signal, namely $3l + \not{E}_T$ comes from $pp \to \widetilde{\chi}_1^\pm \widetilde{\chi}_2^0$, since the production of the heavier neutralinos like $\widetilde{\chi}_3^0$ or $\widetilde{\chi}_4^0$ is highly suppressed. It may be recalled that $\widetilde{\chi}_1^\pm$ and $\widetilde{\chi}_2^0$ masses are degenerate in this

case and are controlled by the soft breaking mass M_2 for the SU(2) gauginos while the masses of $\widetilde{\chi}_3^0$ and $\widetilde{\chi}_4^0$ are governed by the higgsino mass parameter μ with $\mu >> M_2$. This degeneracy holds for all $m_{\widetilde{\chi}_1^\pm}$ to a very good approximation.

Masses and cross-sections	P1			P2			P3		
	Model			Model			Model		
	Wino	Mixed	Higgsino	Wino	Mixed	Higgsino	Wino	Mixed	Higgsino
$m_{\widetilde{\chi}_1^0}$	150	150	150	150	150	150	150	150	150
$m_{\widetilde{\chi}_1^\pm}$	200	200	200	300	300	300	650	650	650
$m_{\widetilde{\chi}_2^0}$	201	210	219	300	304	304	650	651	652
$m_{\widetilde{\chi}_3^0}$	421	269	221	604	370	312	1256	722	657
$\sigma_{(pp \to \widetilde{\chi}_1^\pm \widetilde{\chi}_2^0)}$	0.7	0.43	0.194	0.129	0.083	0.037	0.00207	0.00135	6.9×10^{-4}
$\sigma_{(pp \to \widetilde{\chi}_1^\pm \widetilde{\chi}_3^0)}$	10^{-3}	0.06	0.209	10^{-4}	0.011	0.037	-	0.00022	6.63×10^{-4}
σ_{Total}	0.70	0.49	0.403	0.129	0.094	0.074	0.00207	0.00157	0.00135

Table 2: Table showing the relevant masses and the cross-sections for three parameter points P1, P2 and P3. Here all the masses are in GeV and cross-sections are in pb.

In contrast, the *higgsino models* are characterized by $\mu << M_2$. As a result, $\widetilde{\chi}_2^0$ and $\widetilde{\chi}_3^0$ are nearly mass-degenerate with $\widetilde{\chi}_1^\pm$ where all masses are essentially determined by μ. The degeneracy is more exact as $m_{\widetilde{\chi}_1^\pm}$ increases. Here both $\widetilde{\chi}_1^\pm \widetilde{\chi}_2^0$ and $\widetilde{\chi}_1^\pm \widetilde{\chi}_3^0$ production cross-sections are significant. In spite of this, the total chargino - neutralino production cross-section is smaller than that in a generic *wino model* with similar chargino and neutralino masses. In the *mixed models* ($\mu \approx M_2$), the cross-sections typically have intermediate values with respect to those of the *wino* and the *higgsino models*. The $\widetilde{\chi}_1^\pm$ and $\widetilde{\chi}_2^0$ are nearly degenerate and the degree of degeneracy increases as $m_{\widetilde{\chi}_1^\pm}$ increases. There is always a much larger mass difference between $\widetilde{\chi}_2^0$ and $\widetilde{\chi}_3^0$ compared to the *higgsino model*. It may be noted that these features are independent of M_1, the $U(1)$ gaugino mass, as long as the LSP is bino-dominated, i.e, $M_1 << M_2, \mu$. The choice of $\tan\beta$, the ratio of the Higgs vacuum expectation values, only has a marginal impact.

Production of $\widetilde{\chi}_1^\pm - \widetilde{\chi}_2^0/\widetilde{\chi}_3^0$ occurs through the process $q_i\bar{q}_i'/q_i'\bar{q}_i \to \widetilde{\chi}_1^\pm \widetilde{\chi}_{2,3}^0$, where q and q' for the first two generations ($i = 1, 2$) refer to up and down type of quarks respectively. When the first two generations of squarks are heavy, s-channel W boson exchange becomes the dominant

production process. We note that the $W^{\pm} - \widetilde{\chi}_1^{\pm} - \widetilde{\chi}_{2,3}^0$ coupling is contributed by terms involving products of wino components as well as terms having products of higgsino components of the relevant electroweakinos. The former terms typically dominate over the latter. Thus, as we move from the *wino model* to the *higgsino model*, the gradually diminishing wino contents of $\widetilde{\chi}_1^{\pm}$ and $\widetilde{\chi}_{2,3}^0$ render smaller and smaller cross-sections for $\widetilde{\chi}_1^{\pm} - \widetilde{\chi}_2^0/\widetilde{\chi}_3^0$ production.

The above features are illustrated by Table 2. Here the LSP mass is fixed at 150 GeV. The parameters M_2 and μ are differently chosen in the three models, in particular, $\mu = 2M_2$ (wino), $\mu = M_2/2$ (*higgsino*) and $\mu \simeq M_2$ (*mixed*). Throughout this paper we shall present the numerical results with these characteristic choices. It follows from Table 2 that for a wide range of the chargino mass the total chargino - neutralino production cross-section in the *higgsino (mixed) model* is 60-65% (70-75%) of that in the *wino model*. All next to leading order (NLO) cross-sections are calculated with PROSPINO 2.1 [42]. The reduction in the production cross-section is one of the reasons for relaxed mass limits in the *higgsino* and *mixed models*. However, the LHC mass limits are also sensitive to the choice of the slepton sector which will be addressed in Secs. 4, 5 and 6.

3 The Methodology

In this section we summarize the constraints that we use to restrict the parameter spaces of several *higgsino* and *mixed models*. We also present brief sketches of the simulation using PYTHIA (v6.428) as well as the procedure for scanning the parameter space.

3.1 The Constraints

The three entries listed below are characterized by relatively small theoretical/experimental uncertainties and they constitute what we call the three major constraints.

1. The LHC constraints from the chargino-neutralino searches in the trilepton channel used in this paper are from the ATLAS conference report [43] with $\mathcal{L} = 20$ fb^{-1} data, which is the source of the published paper [16]. Similarly, for the constraints in the slepton sector we use the conference report [44]. It may be noted that there is no major difference in the exclusion contours among the published versions and their predecessors. The ATLAS collaboration quotes the upper limits on the number of events in any new physics model

at 95% CL subject to different sets of selection criteria (see the next subsection). We have simulated the trilepton signal using the same sets of kinematical selections at the generator level using PYTHIA (v6.428) for the *higgsino* and *mixed models* analysed in this paper. The model independent limits then enable us to sketch the exclusion contours in the $m_{\widetilde{\chi}_1^\pm} - m_{\widetilde{\chi}_1^0}$ plane in different models for representative choices of the other parameters as detailed in the following sections. As already noted in the introduction the slepton constraints hardly depend on the composition of the charginos and neutralinos heavier than the sleptons. We have, therefore, directly used the exclusion contours from light L and LR slepton searches in the corresponding *wino models* obtained in [24].

2. The anomalous magnetic moment of the muon ($a_\mu = \frac{1}{2}(g-2)_\mu$) [45] is an important probe for new physics beyond the standard model (SM). There is a significantly large deviation (more than 3σ) of the SM prediction [46,47] from the experimental data [35]. Contributions to $a_\mu^{\rm SM}$ can be categorized into three parts : a part coming from pure quantum electrodynamics, electroweak contributions and a hadronic part. SUSY contributions to a_μ, namely $a_\mu^{\rm SUSY}$, scale with $\tan\beta$. It can also be large when chargino, sneutrino, neutralino and smuons are light [48]. Thus, it is possible to constrain the SUSY parameter space effectively with given upper and lower limits of $\Delta a_\mu = a_\mu^{\rm exp} - a_\mu^{\rm SM}$. The deviation of the experimental data from the SM calculation amounts to [47]

$$\Delta a_\mu = a_\mu^{\rm exp} - a_\mu^{\rm SM} = (29.3 \pm 9.0) \times 10^{-10}. \tag{1}$$

A partial list of analyses regarding $a_\mu^{\rm SUSY}$ in SUSY models is provided by Refs. [48–51]. With the Higgs mass at 125 GeV and stringent lower bounds on squark-gluino masses coming from the LHC, simplified models like mSUGRA have become rather inefficient to accommodate the $(g-2)_\mu$ anomaly [52]. However, non-universal models can still successfully explain the above range of Δa_μ [53]. It should be noted that the $(g-2)_\mu$ constraint is able to impose definite upper and lower bounds on the sparticle masses [54].

3. Following Ref. [24], relic density limits from the WMAP/PLANCK [29,30] is taken as,

$$0.092 < \Omega_{\widetilde{\chi}} h^2 < 0.138. \tag{2}$$

Apart from the above direct constraints we will further analyze our results in relation to the following dark matter detection limits.

- The direct detection bound on spin-independent (SI) LSP-proton scattering cross-section $\sigma^{\rm SI}_{\tilde{\chi}p}$ is imposed using the LUX [38] data.
- DM indirect detection constraints like the bounds on spin-dependent (SD) LSP-proton scattering cross-section $\sigma^{\rm SD}_{\tilde{\chi}p}$ and limits on muon flux given by the IceCube [39] are also important in our case.

We use SuSpect version 2.41 [55] for spectra generation and $a_\mu^{\rm SUSY}$ calculation. SUSYHIT [56] is used for obtaining the decay BRs of the sparticles. DM relic density and observables related to its direct and indirect detection are computed using micrOMEGAs version 3.2 [57].

3.2 The Simulation

In Ref. [43] the ATLAS collaboration defined six signal regions (SRs) : SRnoZa, SRnoZb, SRnoZc, SRZa, SRZb and SRZc. Table 1 of Ref. [43] includes the details of the cuts corresponding to each signal region. The corresponding upper limits on the number of new physics events are listed in Table 4 of Ref. [43]. In all models analysed in this paper we simulate the trilepton signal for the above SRs with a given $m_{\widetilde{\chi}_1^\pm}$ by increasing the LSP mass in small steps. Below a certain LSP mass the above ATLAS upperbounds on the number of new physics events are violated for at least one SR. A point on the exclusion contour is determined in this way. On the other hand when $m_{\widetilde{\chi}_1^\pm}$ is varied, all the LSP masses are allowed above a certain $m_{\widetilde{\chi}_1^\pm}$ which is the lower limit on this parameter. The validation of our simulation and other details have been described in Ref. [24]. We use the same setup for the present work.

3.3 Scanning the parameter space

We take the strong sector parameters to be heavy by choosing $M_3 = 2$ TeV and fixing the masses of the first two generations of squarks and the mass (M_A) of the pseudoscalar Higgs boson at 3 TeV. The mass parameters for the third generation of squarks are fixed at 1.2 TeV. The top trilinear parameter A_t is varied in the range -5 TeV $< A_t <$ 5 TeV in order to obtain the lighter Higgs scalar mass to be in the interval $122 < m_h < 128$ GeV. All the other trilinear parameters except A_t are

taken to be zero. A theoretical uncertainty of 3 GeV in the computation of Higgs mass is considered here. This spread in m_h arises from the uncertainties in the higher order loop corrections up to three loops, that due to the top-quark mass, renormalisation scheme, scale dependence etc [58]. The Higgs bosons other than the lightest one are assumed to be decoupled. We perform scan over the parameters M_1, and M_2 in the range 100 GeV-1 TeV. The slepton masses are correlated to $m_{\widetilde{\chi}_1^0}$ and $m_{\widetilde{\chi}_1^\pm}/m_{\widetilde{\chi}_2^0}$ in this work and the nature of correlation are described in the appropriate subsections. Values of the relevant SM parameters are taken as $m_t^{pole} = 173.2$ GeV, $m_b^{\overline{MS}} = 4.19$ GeV and $m_\tau = 1.77$ GeV. Finally, we consider only the positive sign of μ in this analysis.

4 The $\widetilde{\chi}_1^\pm$-Higgsino and $\widetilde{\chi}_1^\pm$-Mixed Models with Light Left and Right Sleptons

In this sequel analysis that extends our previous work [24] on $\widetilde{\chi}_1^\pm$-*wino models* towards $\widetilde{\chi}_1^\pm$-*higgsino* ones we will review a few salient points as well as refer to some figures of the earlier analysis for the sake of clarity and easier understanding of the present work. The analysis of various $\widetilde{\chi}_1^\pm$-*higgsino* and $\widetilde{\chi}_1^\pm$-*mixed models* using the methodology sketched in the last section, will be presented in this and the next two sections.

4.1 A brief review of the Light Wino and light Left and Right Sleptons (LWLRS) model

In the **L**ight **W**ino and light **L**eft and **R**ight **S**leptons (LWLRS) model [24], the L and the R types of sleptons were assumed to be mass degenerate (modulo the D-term contributions) with a common mass : $(x_1\ M_1 + x_2\ M_2)$. Three choices were considered: i) $x_1 = x_2 = 0.5$, ii) $x_1 = 0.25, x_2 = 0.75$ and iii) $x_1 = 0.75, x_2 = 0.25$, with the slepton mass lying between M_1 and M_2. The models with $x_1 \neq x_2$ are referred to as tilted models denoted by the LWLRS$_{\widetilde{\chi}_1^\pm}$(LWLRS$_{\widetilde{\chi}_1^0}$) with the slepton mass closer to the $\widetilde{\chi}_1^\pm$ ($\widetilde{\chi}_1^0$) mass. The ATLAS group did not interpret their data in any form of the LWLRS model. However, as we shall show in the next subsection, some versions of the corresponding *higgsino model* are indeed rather intriguing since they are practically unconstrained by the LHC data.

The impact of the three major constraints (see Secs.1 and 3) on the parameter space of the

LWLRS model for low $\tan\beta$ (= 6) may be seen in Figure 4a of Ref. [24]. For a negligible LSP mass, the acceptable value of $m_{\widetilde{\chi}_1^\pm}$ is above 610 GeV. On the other hand, for higher values of the LSP masses the limits that had been obtained primarily from the trilepton searches earlier, became weaker. There were two branches in the parameter space consistent with the WMAP/PLANCK data [29, 30]. This feature is common to most of the *wino models* with low $\tan\beta$. The fact that relic density limit is satisfied in the upper branch is related to LSP-sneutrino coannihilation. The lower branch is consistent with the relic density limits via LSP pair-annihilation into the Higgs resonance, corresponding to $m_{\widetilde{\chi}_1^0} \approx m_h/2$[9]. In spite of satisfying the DM relic density limits, a large part of the above parameter space corresponding to low $m_{\widetilde{\chi}_1^\pm}$ is disfavoured by the trilepton and slepton searches. This indeed is the case in all the *wino models* with $x_1 = x_2 = 0.5$. However, the constraints from slepton searches are significantly relaxed in the LWLRS$_{\widetilde{\chi}_1^\pm}$ model and one obtains $m_{\widetilde{\chi}_1^\pm} \geq 450$ GeV for negligible LSP masses(see Fig. 6a of Ref. [24]). The results of Ref. [24] derived from slepton searches are being readily adapted in the corresponding *higgsino* or *mixed model* of the present analysis for reasons already discussed in Sec. 1. However, the entire parameter space allowed even by the relaxed constraints from slepton searches is consistent with the $(g-2)_\mu$ data at best at the 3σ level. This tension at low $\tan\beta$ from the $(g-2)_\mu$ constraint exists in all the *wino models* as already been noted [24]. This feature is also shared by the *higgsino models* as we shall see in the following sections.

A choice of a large $\tan\beta$ (= 30) in the LWLRS model hardly changes the LHC constraints, as may be seen in Fig. 4b of Ref. [24]. However, a significant amount of parameter space is discarded because $\tilde{\tau}_1$ becomes the LSP as a result of enhanced degree of Left-Right mixing considering a large value of $\tan\beta$. On the other hand, since $\tilde{\tau}_1$ is significantly lighter than the other sleptons, τ-rich final states deplete a part of the trilepton signal[10]. This depletion, however, is more effective in the parameter space beyond the reach of the LHC Run-I experiments. We should here point out that the small mass difference between $\tilde{\tau}_1$ and $\widetilde{\chi}_1^0$ which results into satisfying DM relic density via LSP-stau coannihilation (see the upper branch of the region allowed by the WMAP/PLANCK data in Fig. 4b of Ref. [24]) makes the tau-tagged signatures difficult to observe. The Higgs resonance

[9] In some of the cases the Higgs resonance region is accompanied by a small Z resonance annihilation branch. However, we will mostly focus on the former in our present analysis.

[10] The potential of final states with multiple τs from $\widetilde{\chi}_1^\pm$ and $\widetilde{\chi}_2^0$ decays as new signals at the LHC was emphasized in Ref. [59] .

region on the other hand disappears due to a vanishingly small higgsino component of $\widetilde{\chi}_1^0$ which severely suppresses the $h\widetilde{\chi}_1^0\widetilde{\chi}_1^0$ coupling at high $\tan\beta$, a generic feature shared by all the *wino models* with a bino-like LSP. As expected the tension with the $(g-2)_\mu$ constraint is relaxed in this high $\tan\beta$ scenario. As a result there is a narrow APS consistent with all the major constraints.

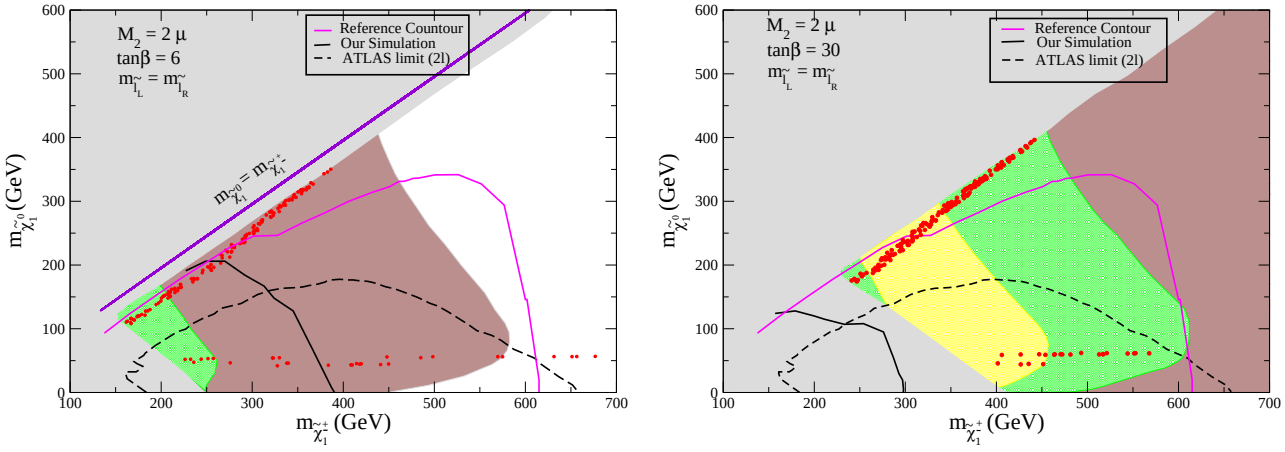
4.2 The Light Higgsino and light Left and Right Sleptons (LHLRS) model

In this subsection we focus on the models characterized by **L**ight **H**iggsino and light **L**eft and **R**ight **S**leptons (LHLRS), where the sleptons are assumed to have masses nearly halfway between the masses of the lightest neutralino and the lighter chargino[11] while $\widetilde{\chi}_1^\pm$ and $\widetilde{\chi}_2^0$ are higgsino-dominated in nature. In this scenario with $M_1 < \mu < M_2$, $m_{\widetilde{\chi}_1^\pm}$, $m_{\widetilde{\chi}_2^0}$ and $m_{\widetilde{\chi}_3^0}$ are close to μ. In this paper we restrict ourselves to the regions of parameter space where the LSP is either bino-dominated ($M_1 << \mu$) or a strong admixture of bino and higgsinos with the former field dominating over the others. In the latter case, the LSP and $\widetilde{\chi}_1^\pm$ are almost mass degenerate.

We do not however include the scenario where the LSP is purely a higgsino or higgsino-dominated ($\mu \lesssim M_1$). In this parameter space all the lighter electroweakinos including the LSP are higgsino-like and nearly mass degenerate. As a result, no interesting LHC signature, except for the well-known monojet + $\not{E}_T$ signal, is expected. DM searches by the LHC collaborations in this channel yielded only null results [60]. However, the results have not been interpreted in terms of the pMSSM scenarios. According to the analysis of Ref. [61] using the LHC Run-I data the bound on the LSP mass in this case is rather weak. Moreover, for the electroweakino mass ranges of current phenomenological importance, the DM is found to be underabundant when $\mu \lesssim M_1$ [62].

In Fig. 1(a), we present the results of the LHLRS analysis for $\tan\beta = 6$. The brown and the green regions signify the parameter space consistent with the $(g-2)_\mu$ constraint at 3σ and 2σ levels respectively. The magenta line represents the reference contour which is the strongest $m_{\widetilde{\chi}_1^0} - m_{\widetilde{\chi}_1^\pm}$ mass limit as obtained in the **L**ight **W**ino and light **L**eft **S**lepton (LWLS) model [see Fig. 1a of Ref. [24]]. The black line is the contour obtained by our simulation for the LHLRS model

[11] Placement of slepton masses follow similar relationship with the masses of the LSP and the lighter chargino as mentioned in the previous subsection. This is also accompanied by similar tilted scenarios like the LHLRS$_{\widetilde{\chi}_1^\pm}$ and LHLRS$_{\widetilde{\chi}_1^0}$ models where sleptons are closer in masses to that of $\widetilde{\chi}_1^\pm$ and $\widetilde{\chi}_1^0$ respectively by specific amounts.



(a) (b)

Figure 1: The brown, green and yellow regions show the parameter space consistent with the $(g-2)_\mu$ constraint at 3σ, 2σ and 1σ level respectively. The magenta line is the reference contour which represents the strongest $m_{\widetilde{\chi}_1^0} - m_{\widetilde{\chi}_1^\pm}$ mass limit as obtained in the **L**ight **W**ino and light **L**eft **S**lepton (LWLS) model [see Fig. 1a of Ref. [24]]. The black line is the contour obtained by our simulation using ATLAS data. The black dashed line represents the exclusion contour from ATLAS slepton searches. The grey region to the left and above the coloured portion of the parameter space is either theoretically discarded or disallowed by our requirement of having a bino-dominated LSP or disallowed for the requirement of $\widetilde{\chi}_1^0$ to be the LSP. The red points satisfy the WMAP/PLANCK data on DM relic density. The $m_{\widetilde{\chi}_1^\pm} = m_{\widetilde{\chi}_1^0}$ line is also shown for the plot in the left panel. For the plot in the right panel, this line does not exist since $\tilde{\tau}_1$ becomes the LSP for $m_{\widetilde{\chi}_1^\pm} \sim m_{\widetilde{\chi}_1^0}$ because of large mixing.

using ATLAS data. The black dashed line represents the exclusion contour from ATLAS slepton searches. The grey region to the left of the APS is theoretically disallowed. The small change in this region compared to that of Fig. 4a of Ref. [24] is due to the choice of a smaller stop mass (here $m_{\widetilde{t}_1} \simeq 1$ TeV, the same in the previous analysis was 2 TeV) and its effect on the electroweak symmetry breaking (EWSB) scale, $Q = \sqrt{m_{\widetilde{t}_1} m_{\widetilde{t}_2}}$, as used in the code SuSpect [55]. The grey region just below the $m_{\widetilde{\chi}_1^\pm} = m_{\widetilde{\chi}_1^0}$ line corresponds to $\mu \lesssim M_1$ which leads to a higgsino-dominated LSP, a scenario kept out of the domain of our analysis for reasons already discussed. The grey region above the aforesaid line is discarded because $\widetilde{\chi}_1^0$ is chosen to be the LSP, a candidate for DM. We should mention that the theoretically disallowed regions which we will often quote in this

work arise from the facts mentioned above. We also take into account the LEP limits [63] for sparticle masses, if necessary.

It is apparent that apart from a small region of the parameter space corresponding to low $m_{\widetilde{\chi}_1^\pm}$, the collider limits are relaxed significantly with respect to the wino dominated scenario (Fig. 4a of Ref. [24]). For negligible $m_{\widetilde{\chi}_1^0}$, a substantially weaker bound ($m_{\widetilde{\chi}_1^\pm} \gtrsim 380$ GeV) compared to the *wino model* is obtained via the trilepton signal. However, the slepton mass limits discard $m_{\widetilde{\chi}_1^\pm}$ up to 600 GeV. On the other hand, with a modestly increased value of $m_{\widetilde{\chi}_1^0}$ such as 150 GeV, the lower bound on $m_{\widetilde{\chi}_1^\pm}$ is about 330 GeV in order to satisfy both the limits from trilepton and slepton searches. For larger LSP masses, the chargino mass bounds are even weaker, as expected, and eventually disappears for $m_{\widetilde{\chi}_1^0} \gtrsim 200$ GeV. In addition to the suppression of the total chargino-neutralino production cross-section as discussed in the Sec. 2, the decrease in the leptonic BRs of the electroweakinos reduces the trilepton signal. For small $m_{\widetilde{\chi}_1^\pm}$, the decays like $\widetilde{\chi}_1^\pm \to W^\pm \widetilde{\chi}_1^0$ and $\widetilde{\chi}_2^0/\widetilde{\chi}_3^0 \to h/Z\ \widetilde{\chi}_1^0$ are kinematically forbidden. Hence, the number of two-body leptonic decays of $\widetilde{\chi}_1^\pm$ and $\widetilde{\chi}_2^0$ remain practically unaltered compared to the *wino model*. Moreover, the lepton pairs from the decays of $\widetilde{\chi}_3^0$ compensate the overall decrease in the cross-section and this leads to almost unchanged LHC limits. The situation changes significantly when the decays $\widetilde{\chi}_1^\pm \to W^\pm\ \widetilde{\chi}_1^0$ and $\widetilde{\chi}_2^0/\widetilde{\chi}_3^0 \to h/Z\widetilde{\chi}_1^0$ are kinematically allowed. The BR($\widetilde{\chi}_1^\pm \to W^\pm\ \widetilde{\chi}_1^0$) being dominant ($\simeq 75\%$), the overall lepton fraction drops down as W-boson decays with the usual small leptonic BRs[12]. Moreover, $\widetilde{\chi}_2^0$ and $\widetilde{\chi}_3^0$ decay dominantly into the gauge/Higgs boson channels, thus depleting the trilepton signal further[13].

Regarding the constraint from $(g-2)_\mu$, the major contribution comes from the neutralino-smuon loop processes. However, the contribution from the chargino-sneutrino loop diagrams are hardly ignorable. In this low $\tan\beta$ scenario of Fig. 1(a), the $(g-2)_\mu$ constraint which typically is satisfied only at the level of 3σ. As expected, the SUSY contribution to $(g-2)_\mu$ falls on the lower side of the 3σ limit rather than on the higher side. In other words, keeping in mind the level of uncertainties of both the SM prediction and the experimental data [45–47], the above 3σ zone is indeed close to the zone where agreement with the experimental data is at higher level of

[12] This happens in spite of the presence of light sleptons which do not couple favourably to the higgsino like $\widetilde{\chi}_1^\pm$ and $\widetilde{\chi}_2^0$.

[13] Numerical values of the relevant BRs for selected BPs will be provided in Sec. 9.

confidence. The situation would change with more accurate SM predictions and more precision in the experimental front. We simply like to comment here that accepting such a relaxed level of the $(g-2)_\mu$ constraint may be worthwhile if there is a scope to open up a region of parameter space having important LHC signature(s). As discussed above, in this 3σ allowed parameter space, the decays $\widetilde{\chi}_1^\pm \to W\widetilde{\chi}_1^0$ and $\widetilde{\chi}_2^0 \to h\widetilde{\chi}_1^0$ would potentially lead to novel collider signatures like $Wh\widetilde{\chi}_1^0$ during the LHC Run-II.

There are two separate branches consistent with the WMAP/PLANCK data in Fig. 1(a). In the parameter space with small slepton masses, bulk annihilation[14] of $\widetilde{\chi}_1^0$ may partly serve as the cause to satisfy the relic density limits via enhanced LSP pair-annihilation. But, this region of the parameter space is disfavoured by the LHC constraints anyway. In the upper branch, μ is close to M_1 so that the bino-like LSP has a sizable higgsino component. Thus, here one finds $\widetilde{\chi}_1^\pm$ mediated LSP pair annihilations to W^+W^- to play a significant role. Annihilation into ZZ, Zh and $t\bar{t}$ through virtual Z exchange open up for higher LSP masses and also contribute significantly. In contrast, the mechanism for satisfying relic density limits in the similar branch of the *wino model* is mainly due to coannihilations of the LSP with stau/sneutrino (see Fig. 4a of Ref. [24]). It is interesting to note that the DM constraint also provides with bounds on the sparticle masses from above since the upper branch ends abruptly above a certain value of $m_{\widetilde{\chi}_1^0}$. This is due to the fact that for large $m_{\widetilde{\chi}_1^\pm}$, the chargino mediated LSP pair annihilation cross-section is suppressed. In addition, the annihilation cross-section to $t\bar{t}$ pairs goes as $(\frac{m_t}{m_{\widetilde{\chi}_1^0}})^2$ [26,64], which becomes inefficient due to increasing value of $m_{\widetilde{\chi}_1^0}$, resulting into over-abundant DM.

The DM relic density satisfied lower branch forming almost a line parallel to the $m_{\widetilde{\chi}_1^\pm}$ axis corresponds to LSP pair-annihilation via s-channel Z/h resonance and it mostly falls on the 3σ zone of the $(g-2)_\mu$ constraint as discussed above. Moreover, a large portion of this line is excluded by slepton searches for relatively low $m_{\widetilde{\chi}_1^\pm}$. The constraints from slepton searches are considerably relaxed in the LHLRS-$\widetilde{\chi}_1^\pm$ model as discussed in Sec. 4.2.

Thus, novel LHC signatures via the decay $\widetilde{\chi}_2^0 \to h\widetilde{\chi}_1^0$ is a potential discovery channel at the LHC (see Sec. 9) provided we accept the 3σ level of agreement with the $(g-2)_\mu$ data.

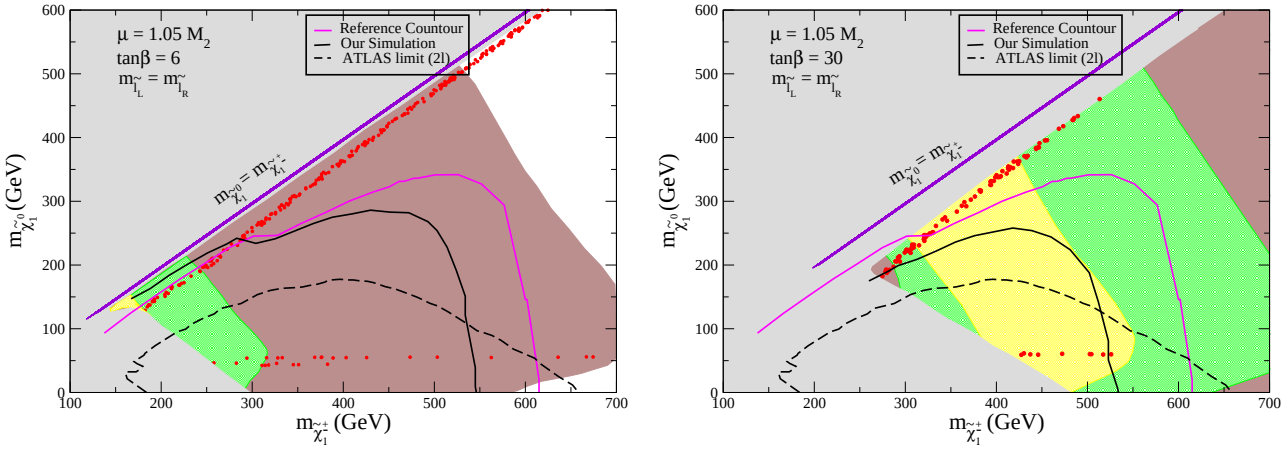
In Fig. 1(b) we present the results for $\tan\beta = 30$. A larger value of $\tan\beta$ causes the lighter stau ($\tilde{\tau}_1$) to become the next to the lightest supersymmetric particle (NLSP) due to larger L-R mixing.

[14] LSP-pair annihilation that occurs via t-channel slepton exchange.

We note that in comparison to a similar wino-dominated $\widetilde{\chi}_1^{\pm}$ scenario like what appears in Fig. 4b of Ref. [24], the theoretically discarded region corresponding to low $m_{\widetilde{\chi}_1^0}$ is smaller in Fig. 1(b). It is partly due to the reasons already discussed for Fig. 1(a). Moreover, μ being relatively low, as demanded by a higgsino dominated $\widetilde{\chi}_1^{\pm}$, the mixing in the stau sector is suppressed. As a result, the portion of the parameter space with stau as the LSP is smaller. No $m_{\widetilde{\chi}_1^{\pm}} = m_{\widetilde{\chi}_1^0}$ line exists in this case as $\tilde{\tau}_1$ becomes the LSP for $m_{\widetilde{\chi}_1^{\pm}} \sim m_{\widetilde{\chi}_1^0}$ because of large mixing. Fig. 1(b) shows further that the LHC exclusion contour from the trilepton data is too small to be of any importance in determining the APS. In fact, the LHC limits are fully encompassed by the theoretically excluded region. In addition to the reasons already discussed, the constraints are also weakened because of a significantly reduced mass of $\tilde{\tau}_1$ in comparison to the same of sleptons of the first two generations. Consequently, there is a significant suppression in the BRs of the decays of $\widetilde{\chi}_1^{\pm}$, $\widetilde{\chi}_2^0$ and $\widetilde{\chi}_3^0$ into states involving e and/or μ. This explains the shrinkage of the LHC forbidden region compared to Fig. 1(a).

The $(g-2)_\mu$ constraint that typically scales with $\tan\beta$ is satisfied much easily in this large $\tan\beta$ scenario even at 1σ level. The largest contribution to $(g-2)_\mu$ is from the neutralino-smuon loop. But the chargino-sneutrino loop also has a significant contribution.

The features of the upper branch allowed by the WMAP/PLANCK data are similar to those in Fig. 1(a). However, since $\tilde{\tau}_1$ is the NLSP in this case stau coannihilation also becomes important for higher LSP masses. Nevertheless, the upper branch is also truncated in this case, thereby imposing an upper limit on the sparticle spectra. This bounded region is consistent with both the $(g-2)_\mu$ and the LHC constraints. We recall that in the wino dominated scenario (see Fig. 4b of Ref. [24]), the Higgs resonance region disappears at large $\tan\beta$ due to vanishingly small higgsino component of $\widetilde{\chi}_1^0$ which severely suppresses the $\mathrm{h}\widetilde{\chi}_1^0\widetilde{\chi}_1^0$ coupling. In contrast, μ being smaller in the present scenario, $\widetilde{\chi}_1^0$, though dominantly a bino, has sufficient higgsino components. Thus, the h-resonance region extends to large values of $m_{\widetilde{\chi}_1^{\pm}}$. The bulk of this region, though allowed by the $(g-2)_\mu$ constraint, is disfavoured by the direct slepton search data. However, as already noted, this region opens up in the LHLRS$_{\widetilde{\chi}_1^{\pm}}$ model.



(a) (b)

Figure 2: Plots in the $m_{\widetilde{\chi}_1^\pm} - m_{\widetilde{\chi}_1^0}$ plane for the LMLRS scenario with $\tan\beta$=6 and 30. Colours and conventions are the same as in Fig. 1.

4.3 The Light Mixed $\widetilde{\chi}_1^\pm$ with light Left and Right Sleptons (LMLRS) model

The analysis of this subsection is based on the **L**ight **M**ixed $\widetilde{\chi}_1^\pm$ with light **L**eft and **R**ight **S**leptons (LMLRS) scenario where the states $\widetilde{\chi}_1^\pm$, $\widetilde{\chi}_2^0$ and $\widetilde{\chi}_3^0$ are admixtures of large wino and higgsino components while the slepton masses are chosen as in the previous subsection. We consider $\mu = 1.05\ M_2$, a choice that corresponds to a large higgsino-wino mixing while keeping $\widetilde{\chi}_1^\pm$, $\widetilde{\chi}_2^0$ and $\widetilde{\chi}_3^0$ to be still dominated by the higgsinos. On the other hand, $\widetilde{\chi}_1^0$ may have a significant amount of higgsino component in some region of parameter space, although it is by and large a bino-dominated state ($\mu > M_1$). We analyze the production processes : $pp \to \widetilde{\chi}_1^\pm\ \widetilde{\chi}_2^0/\widetilde{\chi}_3^0$. In Fig. 2(a), we show our results for $\tan\beta = 6$.

A gradual weakening of the LHC constraint from the trilepton search is evident from the LWLRS model (Fig. 4a of Ref. [24]), to the LMLRS model (Fig. 2(a)) and then to the LHLRS model (Fig. 1(a)) while the higgsino fraction within $\widetilde{\chi}_1^\pm$ increases steadily. This is as expected from the discussions on the cross-sections in Sec. 2.

Thus, for a negligible LSP mass the lighter chargino mass limit that is allowed via the trilepton search is about 550 GeV in Fig. 2(a) compared to about 390 GeV in Fig. 1(a). However, the model independent results of slepton searches push the above limits in the figures to almost an identical value ($\simeq$600 GeV).

Point from Fig.	2a	2a	2b	4b
M_1	270	59	239	316
M_2	342	601	348	374
μ	359	631	365	393
$m_{\widetilde{\chi}_1^0}$	251	57	228	298
$m_{\widetilde{\chi}_1^\pm}$	301	568	315	342
$m_{\widetilde{\chi}_2^0}$	311	569	318	351
$m_{\widetilde{\chi}_3^0}$	369	639	376	403
$\mathcal{M}^D_{\tilde{e},\tilde{\mu}_L}$	284	443	277	327
$\mathcal{M}^D_{\tilde{e},\tilde{\mu}_R}$	284	443	277	2000
$m_{\tilde{\tau}_1}$	278	435	238	327
M_ν^D	274	436	266	318
$\Omega_{\tilde{\chi}} h^2$	0.11	0.098	0.14	0.1
$\sigma_{SI}(pb) \times 10^{-9}$	12	0.078	2.32	9.36
$a_\mu^{\rm SUSY} \times 10^{-10}$	6.5	2.2	34	25

Table 3: The sparticle spectra corresponding to different points chosen from Fig. 2 and Fig. 4. All the masses are in GeV.

We observe that in the small $m_{\widetilde{\chi}_1^\pm}$ region of Fig. 2(a), the limits from the LHC trilepton searches are practically unaltered with respect to the corresponding *wino model* (Fig. 4a of Ref. [24]), in spite of differing wino and higgsino components within $\widetilde{\chi}_1^\pm$ between the two scenarios. Here BR of $\widetilde{\chi}_2^0$ decaying into invisible $\nu\tilde{\nu}$ final state reduces significantly due to an increase in its higgsino fraction. This on the other hand is compensated the reduction in the cross-section via an increase in the leptonic BR leading to an almost unchanged LHC limit. We further note that $\widetilde{\chi}_3^0$ does not contribute to the trilepton signal appreciably since it decays principally via $Z\widetilde{\chi}_1^0$ mode with BR around 80%. Moreover, the production cross-section for $\widetilde{\chi}_3^0\ \widetilde{\chi}_1^\pm$ is rather small compared to $\widetilde{\chi}_2^0\ \widetilde{\chi}_1^\pm$ since $m_{\widetilde{\chi}_3^0}$ is somewhat larger than $m_{\widetilde{\chi}_2^0}$. Some of the above features are illustrated by two representative points taken from Fig. 2(a)) in Tables 3 and 4. In the region of high $m_{\widetilde{\chi}_1^\pm}$, the decay modes $\widetilde{\chi}_2^0 \to h\widetilde{\chi}_1^0$ and $\widetilde{\chi}_1^\pm \to W^\pm\widetilde{\chi}_1^0$ open up (the BRs lie around 10%). $\widetilde{\chi}_3^0$ decays dominantly into $Z\widetilde{\chi}_1^0$ as before but a sizable fraction goes to $h\widetilde{\chi}_1^0$. Thus, the LHC exclusion contour shrinks when

Decay Modes	Point from Fig.				Decay Modes	Point from Fig.			
	2a	2a	2b	4b		2a	2a	2b	4b
$\widetilde{\chi}_2^0 \to \widetilde{l}_L^{\pm} l^{\mp}$	38.4	30	26	44					
$\to \widetilde{\nu}\bar{\nu}$	24	42	28.8	30					
$\to \widetilde{l}_R^{\pm} l^{\mp}$	10	-	2.4	-					
$\to \widetilde{\tau}_1^{\pm} \tau^{\mp}$	18	10	42	26	$\widetilde{\chi}_3^0 \to \widetilde{l}_L^{\pm} l^{\mp}$	0.6	-	-	0.4
$\to \widetilde{\tau}_2^{\pm} \tau^{\mp}$	7.4	6		-	$\to \widetilde{\nu}\bar{\nu}$	5.4	1	3.6	6
$\to \widetilde{\chi}_1^0 h$	-	9	-	-	$\to \widetilde{l}_R^{\pm} l^{\mp}$	0.8	-	-	-
$\to \widetilde{\chi}_1^0 Z$	-	3		-	$\to \widetilde{\tau}_1^{\pm} \tau^{\mp}$	0.6	0.8	34	50
$\widetilde{\chi}_1^{\pm} \to \widetilde{\nu}_{\tau} \tau$	25	16	20	31	$\to \widetilde{\tau}_2^{\pm} \tau^{\mp}$	3.4	2	15	-
$\to \widetilde{\tau}_1 \nu_{\tau}$	9	8.5	32	7	$\to \widetilde{\chi}_1^0 h$		24	0.7	-
$\to \widetilde{\tau}_2 \nu_{\tau}$	1	5	-	-	$\to \widetilde{\chi}_1^0 Z$	89	71	45	42
$\to \widetilde{\nu}_l l$	50	32	32	48					
$\to \widetilde{l}_L \nu_l$	16	26	14.8	14					
$\to W^{\pm} \widetilde{\chi}_1^0$	-	12	1.4						

Table 4: The decay modes and BRs of different points taken from Fig. 2 and Fig. 4.

compared with Fig. 4a of Ref. [24]. These features are illustrated in Table 4.

Regarding $(g-2)_{\mu}$, in all the cases the LHC allowed parameter space is consistent at 3σ level. Both the loops involving neutralinos as well as charginos contribute with comparable magnitudes.

Along the upper red dotted line, the main contribution to the observed relic density are chargino mediated LSP annihilation into the final state W^+W^- and LSP pair annihilation into $t\bar{t}$. Some amount of bulk annihilation is also present for low $m_{\widetilde{\chi}_1^{\pm}}$ although this region of parameter space is discarded by the LHC constraints. Unlike the *higgsino model* of Fig. 1(a) the upper branch does not end abruptly (at $m_{\widetilde{\chi}_1^{\pm}} \approx 400$ GeV). This is due to the fact that $\widetilde{\chi}_1^0 - \widetilde{\chi}_1^{\pm} - W^{\pm}$ coupling which is behind the $\widetilde{\chi}_1^{\pm}$ mediated annihilation to W^+W^- is stronger because of larger wino content of the LSP in the *mixed model*. In the corresponding *wino model* (Fig. 4a of Ref. [24]), however, the relic density falls within the observed range mainly due to stau/sneutrino coannihilations. The lower branch of red points consistent with the observed DM relic density arises through Z/h resonance.

Fig. 2(b) illustrates the results for $\tan\beta = 30$. The small change in the theoretically discarded

region is due to reasons explained earlier (see Sec. 4.1). Here the parameter space excluded by the LHC constraint shrinks with respect to that in the *wino model* (Fig. 4b of Ref. [24]). The reasons are the same as the ones discussed in the context of Fig. 2(a) and 1(b). However, $\widetilde{\chi}_3^0$ decay has no bearing on the LHC limits in this case. Significantly larger parameter spaces consistent with the $(g-2)_\mu$ constraint at the level of 1σ and 2σ are available in this high $\tan\beta$ scenario. On the other hand, for the DM constraint as satisfied in the the upper red dotted branch, the main DM producing mechanisms are stau-LSP coannihilation and stau-stau annihilation as in the *wino model* (Fig. 4b of Ref. [24]). Chargino-mediated annihilation and annihilation into $t\bar{t}$ pairs are also present albeit to a lesser extent. The features of one representative point in this parameter space is illustrated in Tables 3 and 4. Here the Higgs resonance strip extends to higher $m_{\widetilde{\chi}_1^\pm}$ compared to the *wino model* (see Fig. 4b of Ref. [24]) where it was practically absent. This is due to a modest increase in the higgsino component of the LSP. However, this parameter space is strongly disfavoured by the LHC limits even in the LMLRS$\widetilde{\chi}_1^\pm$ model.

We end this section by noting that in both the LHLRS and LMLRS models with high $\tan\beta$ we obtain several APSs consistent with the main constraints.

5 The Higgsino and Mixed Models with Light Left Sleptons

5.1 A brief review of the Light Wino and light Left Sleptons (LWLS) model

We recall that in Fig. 1 of our previous analysis (Ref. [24]), the model characterized by **L**ight **W**ino and light **L**eft **S**leptons (LWLS) yields the strongest mass limit on $\widetilde{\chi}_1^\pm$. For negligible $m_{\widetilde{\chi}_1^0}$, $m_{\widetilde{\chi}_1^\pm}$ ranging up to 610 GeV is excluded. In all cases the low $\tan\beta$ scenarios are consistent with the $(g-2)_\mu$ constraint at best at the 3σ level. On the other hand, for large $\tan\beta$, the SUSY prediction has a better agreement with constraint which is satisfied at 1σ or 2σ levels. In all cases the parameter space consistent with the WMAP/PLANCK data has two limbs. In the upper limb various coannihilations lead to the desired relic density. The lower limb which represents the LSP pair annihilation through the h-resonance is either absent or strongly disfavoured by the LHC constraints in the high $\tan\beta$ scenarios.

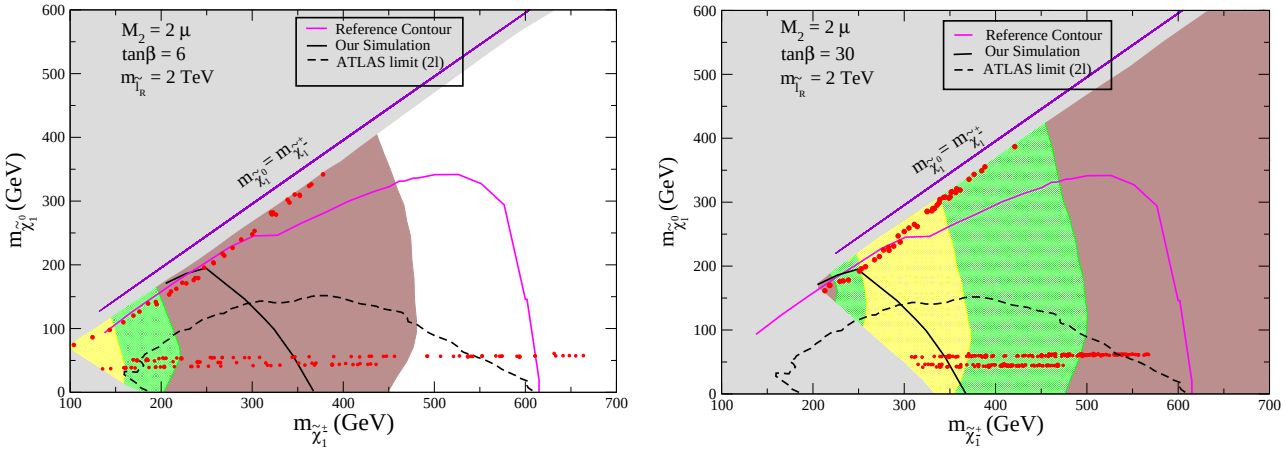
5.2 The Light Higgsino and light Left Sleptons (LHLS) model

In this section we replace *wino* of the previous subsection by a *higgsino* and focus on models with **L**ight **H**iggsino and light **L**eft **S**leptons (LHLS) where $\widetilde{\chi}_1^{\pm}$ and $\widetilde{\chi}_2^0$ are higgsino-dominated and left slepton masses are kept midway between $m_{\widetilde{\chi}_1^{\pm}}$ and $m_{\widetilde{\chi}_1^0}$. Right sleptons are taken to be heavy.

Fig. 3(a) shows our results for the model with $\tan\beta = 6$. If we compare this with Fig. 1a of Ref. [24] we see that the theoretically discarded regions are almost the same in both cases. The small change is due to a different choice of EWSB scale as noted earlier. The LHC limits from the trilepton searches are significantly degraded in the *higgsino* case. The reasons are the same as the ones in Sec. 4.2. For low LSP masses, however, one finds a region with $m_{\widetilde{\chi}_1^{\pm}} \gtrsim 600$ GeV to be allowed from slepton search. This limit will be relaxed to 410 GeV in the tilted LHLS$_{\widetilde{\chi}_1^{\pm}}$ models (See [24] Figs. 3a and 3b).

The major contribution to $(g-2)_\mu$ comes from the chargino-sneutrino loop as expected in models with light L-type sleptons (see Ref. [24] for details). The $(g-2)_\mu$ allowed regions at the level of 1σ, 2σ and 3σ are similar to those of Fig. 1a of Ref. [24]. The observations regarding the points satisfying the WMAP/PLANCK limits are similar to those of Fig. 3(a) i.e. the lower red dotted branch comes from Z/h resonance annihilation and the upper branch from annihilation to W^+W^-, $t\bar{t}$, ZZ pairs. There is a small amount of sneutrino coannihilation in the upper branch along with a little bulk annihilation for very low $m_{\widetilde{\chi}_1^{\pm}}$ disfavoured by the LHC bounds. The reasons for the abrupt end of the upper branch indicating upper bounds on $m_{\widetilde{\chi}_1^{\pm}}$ and $m_{\widetilde{\chi}_1^0}$ are already discussed in Sec. 4.2. The $(g-2)_\mu$ constraint is satisfied only at the level of 3σ.

Our results for $\tan\beta = 30$ is shown in Fig. 3(b). The collider exclusion limit is the same as that of Fig. 3(a). Since the right sleptons are heavy, there is no large mixing in the stau sector. As a result, the LHC exclusion contour remains unaltered in spite of the change in $\tan\beta$. The dominant contribution to $(g-2)_\mu$ comes from the chargino-sneutrino loop diagram and it is characteristically similar to Fig. 3(a) except that there is the usual $\tan\beta$ enhancement leading to valid 1σ and 2σ regions. Annihilation and coannihilation mechanisms of the LSP in the regions satisfying the WMAP/PLANCK constraints in this scenario are similar to those of Fig. 3(a). The LSP pair annihilation into the Higgs resonance is allowed in the LHLS$\widetilde{\chi}_1^{\pm}$ model.



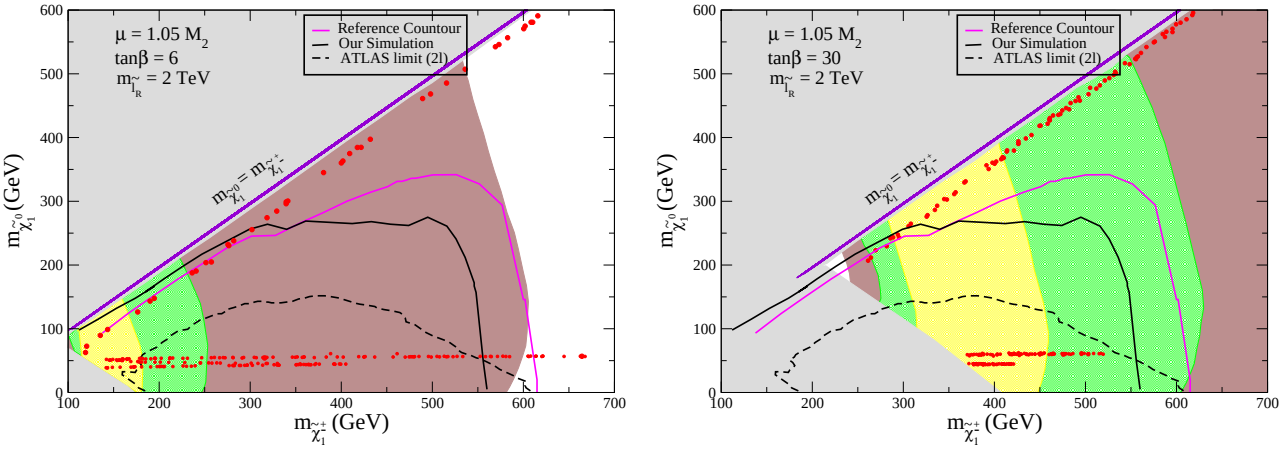
(a) (b)

Figure 3: Plots for the LHLS model with $\tan\beta$= 6 (a) and 30 (b). Colours and conventions are the same as in Fig. 1(a).

5.3 The Light Mixed $\widetilde{\chi}_1^{\pm}$ and light Left Sleptons (LMLS) model

In Fig. 4(a) we show our results for the **L**ight **M**ixed $\widetilde{\chi}_1^{\pm}$ and light **L**eft **S**leptons model (LMLS) with $\tan\beta$= 6. The collider exclusion contour is weakened compared to the reference contour of Fig. 1a of Ref. [24]. The reasons are almost same as those mentioned in the discussions for Fig. 2(a). Major contribution to $(g-2)_\mu$ is provided by the chargino-sneutrino loop diagram. The points satisfying the WMAP/PLANCK limits in the lower branch arise as a result of Z/h resonance annihilation processes. For the upper branch, main mechanisms are annihilations into W^+W^-, ZZ, $t\bar{t}$ pairs.

Fig. 4(b) shows the results for large $\tan\beta$ in the LMLS scenario. The observations regarding the upper limb consistent with the WMAP/PLANCK constraints are similar to those of Fig. 4(a). As in all high $\tan\beta$ scenarios there are portions of the parameter space consistent with the $(g-2)_\mu$ constraint at 1σ and 2σ levels leading to an APS consistent with all the major constraints. We show the features of one representative point for this scenario in Tables 3 and 4.



(a) (b)

Figure 4: Plots for the LMLS model with tan β=6 (a) and 30 (b). Colours and conventions are the same as in Fig. 1(a).

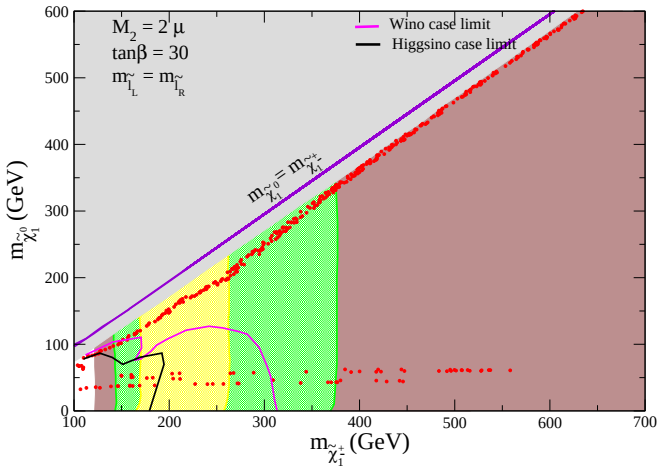


Figure 5: Plot for the LHHS scenario with tanβ =30. The magenta line represents the exclusion contour at 8 TeV by the ATLAS collaboration [43] for the *wino model*. The black line stands for the much weaker exclusion contour in the corresponding *higgsino model* obtained by our simulations. Other colours and conventions are the same as in Fig. 1(a).

6 The Light Higgsino and Heavy Sleptons (LHHS) model

In the **L**ight **H**iggsino and **H**eavy **S**leptons (LHHS) scenario the chargino decays to W$\widetilde{\chi}_1^0$ with 100% BR and the decay $\widetilde{\chi}_2^0 \to Z\widetilde{\chi}_1^0$ has 100% BR for $(m_{\widetilde{\chi}_2^0} - m_{\widetilde{\chi}_1^0}) < m_h$. For larger $m_{\widetilde{\chi}_2^0}$, the mode $\widetilde{\chi}_2^0 \to h\widetilde{\chi}_1^0$ opens up and its BR can be $\approx 40\%$ near threshold. With increasing value of $m_{\widetilde{\chi}_2^0} - m_{\widetilde{\chi}_1^0}$, the BR($\widetilde{\chi}_2^0 \to h\widetilde{\chi}_1^0$) may be as large as 60%. The presence of this mode is the main difference with the LWHS scenario and leads to the $(W + h + \not{E}_T)$ signal. The BR of the mode $\widetilde{\chi}_3^0 \to Z\widetilde{\chi}_1^0$ is around 70%. However, the LHC limits in this case are degraded due to a reduction in cross-section as already discussed. For $m_{\widetilde{\chi}_1^\pm} > 200$ GeV, all the LSP masses are allowed. On the other hand, for negligible LSP masses, a weaker limit ($m_{\widetilde{\chi}_1^\pm} \gtrsim 175$ GeV) is obtained.

The above features, and, consequently the LHC exclusion contours, are fairly independent of $\tan\beta$. However, as already shown in the last two sections, the constraints from $(g-2)_\mu$ is effective for high $\tan\beta$. This is particularly true in a situation with heavy slepton masses that potentially reduces $a_\mu^{\rm SUSY}$. Thus, only the case of $\tan\beta = 30$ is shown in Fig. 5. The SUSY contribution to $(g-2)_\mu$ is dominated by the chargino-sneutrino loop diagram. The upper branch of the region consistent with the WMAP/PLANCK data arises due to chargino-mediated LSP pair annihilation to W pairs. There is also annihilation to fermion anti-fermion pairs through virtual Z exchange and some amount of LSP-chargino coannihilation. The Z/h-resonance region is also allowed in this scenario by the major constraints and the $(g-2)_\mu$ constraint is satisfied even at the level of 1σ.

An analogous case of a Light Mixed and Heavy Sleptons (LMHS) scenario would have the corresponding LHC exclusion contour lying in between the magenta and the black lines of Fig. 5. This is expected from the chargino-neutralino production cross-sections as discussed in Sec. 2. We do not present the details here since no qualitatively new feature of the signal emerges from this analysis.

7 Direct Detection via Spin-independent scattering

Spin-independent (SI) interaction of the lightest neutralino with quarks inside the detector nucleus occurs via s-channel squark exchange and t-channel Higgs exchange processes. With the present LHC bounds squarks are considerably heavy. Hence, the Higgs exchange diagrams would dominantly contribute towards $\sigma_{p\chi}^{SI}$, the spin-independent $\tilde{\chi} - p$ scattering cross-section [65]. In this

context we note that the $h(H)\widetilde{\chi}_1^0\widetilde{\chi}_1^0$ coupling involves products of the gaugino and the higgsino components of the neutralino diagonalizing matrix [3]. Unless $|M_1 - |\mu|| \lesssim M_Z$, in the Higgs decoupling zone [3] satisfying $m_H \simeq m_A >> M_Z$, the Higgs couplings to a bino-dominated LSP is approximately given as below [66].

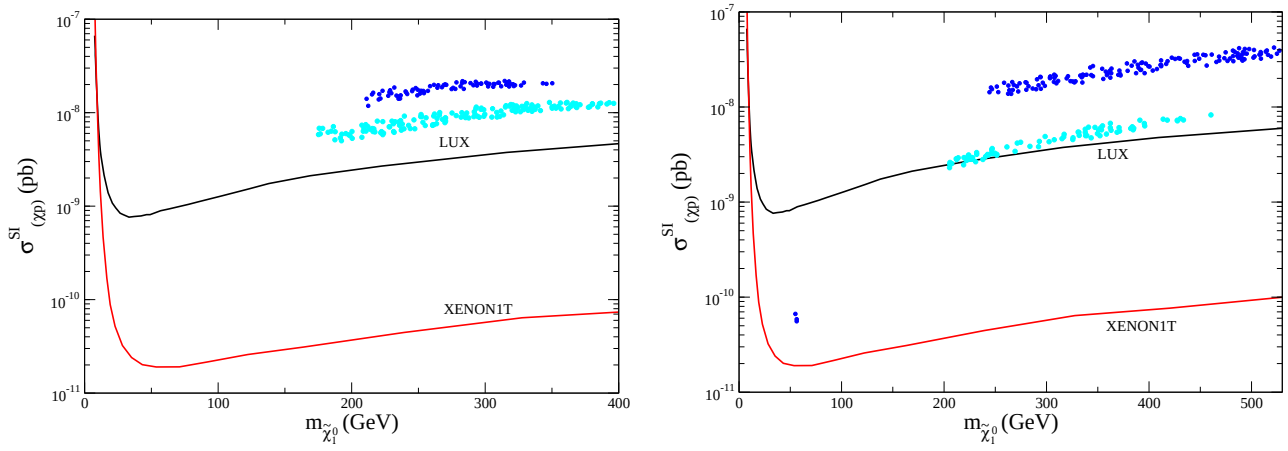
$$\begin{aligned} C_{h\tilde{\chi}\tilde{\chi}} &\simeq \frac{m_Z s_W t_W}{M_1^2 - \mu^2}[M_1 + \mu \sin 2\beta], \\ C_{H\tilde{\chi}\tilde{\chi}} &\simeq -\frac{m_Z s_W t_W}{M_1^2 - \mu^2}\mu \cos 2\beta. \end{aligned} \tag{3}$$

Here $s_W = \sin\theta_W$ etc. with θ_W as the Weinberg angle. Similar results for a wino or a higgsino-dominated LSP may be seen in Ref. [66]. Clearly, the above shows that the SI cross-section $\sigma_{p\chi}^{SI}$ would be large when there is a significant amount of bino-higgsino mixing i.e. $M_1 \simeq \mu$. This is unlike a pure gaugino or a pure higgsino DM when the associated SI cross-section would become quite small. We note that in contrast to our previous analysis [24], where we considered a bino dominated LSP with $\mu >> M_1, M_2$, the present work has a significant amount of higgsino component in the LSP. As a result, $\sigma_{p\chi}^{SI}$ is typically larger than what was seen in Ref. [24] and in most of the cases its values lie above the LUX [38] limit. However, we must note that there still exists a significant amount of uncertainty in the theoretical estimate of the SI cross-section (for a brief discussion see Ref. [24] and references quoted therein). This at least relates to issues like uncertainties in the determination of the strangeness content of nucleon, local DM density and velocity distribution profiles. All these uncertainties may accommodate lowering of the cross-section by an order of magnitude. We will present our results in the following subsections for the *higgsino* and the *mixed models*. We like to point out that no tilted scenarios have been included in our analyses on direct and indirect detection of dark matter.

7.1 LHLRS and LMLRS

The results for the SI direct detection are shown in Fig. 6(a) and Fig. 6(b) corresponding to i) higgsino-dominated $\widetilde{\chi}_1^\pm$ (LHLRS) and ii) wino-higgsino mixed $\widetilde{\chi}_1^\pm$ (LMLRS) analyses of Fig. 1 and Fig. 2 respectively. Fig. 6(a) combines the results in the $m_{\widetilde{\chi}_1^0} - \sigma_{p\chi}^{SI}$ plane corresponding to two values of $\tan\beta$ (blue and cyan for $\tan\beta = 6$ and 30 respectively) as used in Fig. 1(a) and Fig. 1(b). Similarly, Fig. 6(b) details the results corresponding to Fig. 2(a) and Fig. 2(b) for the same values

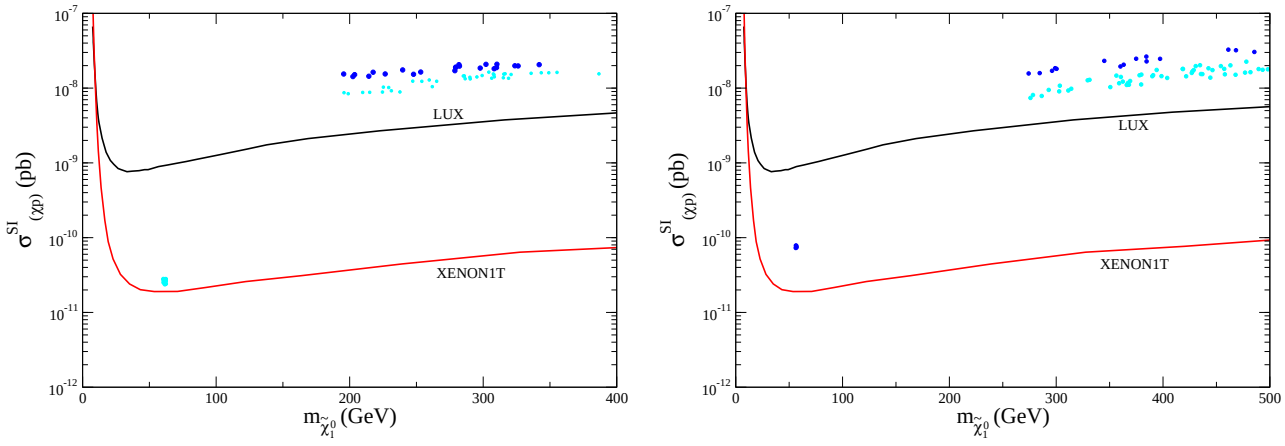
of $\tan\beta$ as mentioned above. Figs. 6(a) shows only the allowed points that satisfy the relic density limits, the $(g-2)_\mu$ constraint (upto 2σ for large $\tan\beta$, and 3σ for small $\tan\beta$ cases) and the collider limits for $m_{\tilde{\chi}_1^0}$ between 200 and 350 GeV. $\sigma_{p\chi}^{SI}$ for the points exceed the LUX limit, while staying within an order of magnitude of the same limit[15]. In regard to the *mixed model* (Fig. 6(b)), we similarly find that parameter zones satisfying $m_{\tilde{\chi}_1^0} > 200$ GeV are consistent with the major constraints. Here also the points exceed the LUX limit by a similar amount. This is unlike the analysis of the LWLRS scenario of Ref. [24] where it was not difficult to satisfy the LUX limit. Since the parameter points correspond to a deviation below an order of magnitude from the LUX limit, we consider them to be presently acceptable in view of the uncertainties discussed before. There are a few points in the Higgs resonance region for the low $\tan\beta$ case. Since Higgs-pole annihilation occurs for $m_{\tilde{\chi}_1^0} \sim \frac{M_h}{2}$ and the allowed points from this region correspond to very high $m_{\tilde{\chi}_1^\pm}$ (see Fig. 2(a)), the LSP in this region is highly bino-dominated, thus having very small values of $\sigma_{p\chi}^{SI}$. The XENON1T experiment will conclusively probe these models.



(a) (b)

Figure 6: Direct detection results for the LHLRS (a) and LMLRS (b) scenarios with $\tan\beta = 6$ (blue) and 30 (cyan). The LUX and XENON1T limits are shown as black and red lines respectively. The points satisfying the WMAP/PLANCK and LHC limits are shown. The $(g-2)_\mu$ constraint is applied up to the level of 3σ for low and 2σ for high $\tan\beta$ cases respectively.

[15]This is especially so for models with high $\tan\beta$ which are also in better agreement with the $(g-2)_\mu$ constraint.



(a) (b)

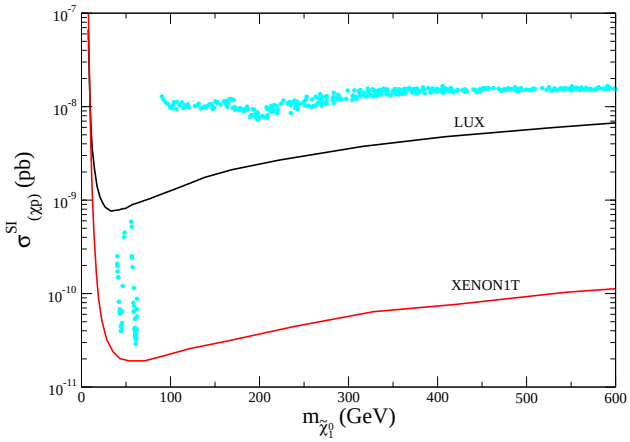
Figure 7: Direct detection results for the LHLS (a) and LMLS (b) scenarios with $\tan\beta = 6$ (blue) and 30 (cyan). Colours and conventions are the same as in Fig. 6.

The results for the SI direct-detection are shown in Fig. 7(a) and Fig. 7(b) corresponding to the LHLS and LMLS scenarios for the analyses of Fig. 3 and Fig. 4 respectively. The colours (blue and cyan for low and high values of $\tan\beta$ as used in Figs. 3(a) and 3(b) respectively) and conventions used in Fig. 7(a) are the same as in Fig. 6(a). Fig. 7(a) shows only the points satisfying the major constraints, which in this case, lie in the range 200 GeV$< m_{\widetilde{\chi}^0_1} <$ 350 GeV. On the other hand, Fig. 7(b), which corresponds to Fig. 4(a) and Fig. 4(b), shows the above type of allowed points for $m_{\widetilde{\chi}^0_1} > 300$ GeV. These points give rise to $\sigma^{SI}_{p\chi}$ the LUX limit by a similar amount as before. There are a few points in both the figures, lying in the Higgs resonance region which are still allowed by all the major constraints. This region of parameter space, having very small values of $\sigma^{SI}_{p\chi}$, will be fully explored by the XENON1T experiment in future.

7.3 LHHS

The results for the SI direct-detection are shown in Fig. 8 corresponding to a scenario of a higgsino-dominated $\widetilde{\chi}^{\pm}_1$ for the LHHS analysis of Fig. 5 with $\tan\beta = 30$. In the LHHS analysis we consider masses of the left and the right sleptons to be larger than $m_{\widetilde{\chi}^{\pm}_1}$ by 200 GeV while a choice of $M_2 = 2\mu$ is made to have higgsino-domination in $\widetilde{\chi}^{\pm}_1/\widetilde{\chi}^0_2$. The LSP is however bino-dominated because of the choice $M_1 < \mu$. Fig. 8 shows only the allowed points that satisfy the main constraints.

Parameter points with $m_{\widetilde{\chi}_1^0}$ above 80 GeV satisfy these criteria. The same is true for a small region around Higgs pole annihilation zones i.e. $m_{\widetilde{\chi}_1^0} \simeq \frac{M_h}{2}$. $\sigma_{p\chi}^{SI}$ for the parameter points with $m_{\widetilde{\chi}_1^0}$ above 80 GeV exceed the LUX limit but they are still within an order of magnitude. On the other hand, the allowed points in the Higgs resonance region lie much below the LUX limit in a region to be conclusively probed by the XENON1T experiment in near future.



(a)

Figure 8: Direct detection results for the LHHS scenario with $\tan\beta = 30$ for higgsino dominated $\widetilde{\chi}_1^{\pm}$ scenario. The LUX and XENON1T limits are shown as black and red lines. The points allowed by the WMAP/PLANCK and collider constraints are shown. The $(g-2)_\mu$ constraint is applied up to the level of 3σ.

8 Spin-dependent (SD) direct detection cross-section and indirect detection reach for muon flux

A larger higgsino content of the LSP, as explored in this analysis, can potentially be interesting for indirect detection of DM. This is principally due to a larger spin-dependent $\tilde{\chi} - p$ scattering cross-section $\sigma_{p\chi}^{SD}$ which results from a large $Z\tilde{\chi}\tilde{\chi}$ coupling $C_{Z\tilde{\chi}\tilde{\chi}} = |N_{13}^2 - N_{14}^2|$, where N_{ij} refers to the elements of the neutralino diagonalizing matrix. The coupling $C_{Z\tilde{\chi}\tilde{\chi}}$ is a measure of higgsino asymmetry. Thus, on one hand, $\sigma_{p\chi}^{SI}$ is already large because μ and M_1 are not too far away from

each other. On the other hand, $\sigma_{p\chi}^{SD}$ is also in the larger side due to increased amounts of higgsinos within the LSP. The above enhancement in the scattering cross-sections of both the types in turn causes a loss of energy of a DM particle so that their velocities may go below the escape velocity. This results into gravitational capture of DM within the dense region of an astrophysical object. The captured LSPs then undergo pair annihilations. Because of an increased higgsino content within the LSP, the pair annihilations may lead to highly energetic neutrinos within the Sun. The resulting muon flux out of the charged current interactions from the neutrinos coming from the Sun may effectively be probed at the IceCube [39, 40] experiment. In SUSY, neutralino annihilations at tree level would not produce neutrinos. However, the latter may arise from gauge bosons, heavy quarks, τ-leptons etc. The neutrinos may thus have a broad energy distribution with the energy being limited to an appreciable fraction of the mass of the LSP. Neutrinos from $b\bar{b}$ or $\tau^+\tau^-$ are the primary channels when the LSP is lighter than M_W. However, due to a large threshold, the above neutrinos may not be suitable for detection. For massive neutralinos, LSP pair annihilation would produce gauge bosons, top quarks or Higgs bosons. A neutralino having a significant amount of higgsinos may pair annihilate to produce gauge bosons. This, in turn, may become a suitable source for high energy neutrinos.

In order to estimate the capture cross-section in relation to the DM annihilation cross-section for the Sun, one considers the time evolution of N DM particles,

$$\frac{dN}{dt} = C - C_A N^2. \tag{4}$$

Here C measures the rates at which DM particles are captured. C_A relates to the strength of depletion due to DM annihilation. The annihilation rate Γ_A in turn is related to C_A via $\Gamma_A = \frac{1}{2} C_A N^2$ [27, 67, 68].

Solution of Eq.4 results into $\Gamma_A \equiv \frac{1}{2} C_A N^2 = \frac{1}{2} C \tanh^2(t/\tau)$ where $\tau = 1/\sqrt{C C_A}$. Within the MSSM and for objects like the Sun (that would correspond to large annihilation and large capture rates) one finds that for the Solar age of $t = t^{\odot} = 4.5 \times 10^9$ years, it is justified to assume $t/\tau >> 1$. This leads to $\Gamma_A = \frac{1}{2} C$, an equilibrium scenario out of capture and annihilation [69]. However, this is hardly possible for a less massive object like the Earth for which a captured LSP would have a much smaller escape velocity and where one has dominance of the spin-independent interactions in the DM-nuclear scattering. This leads to a weaker indirect detection signal in general [27]. In contrast to the above, the Sun is a massive object with a much larger escape velocity for the LSP.

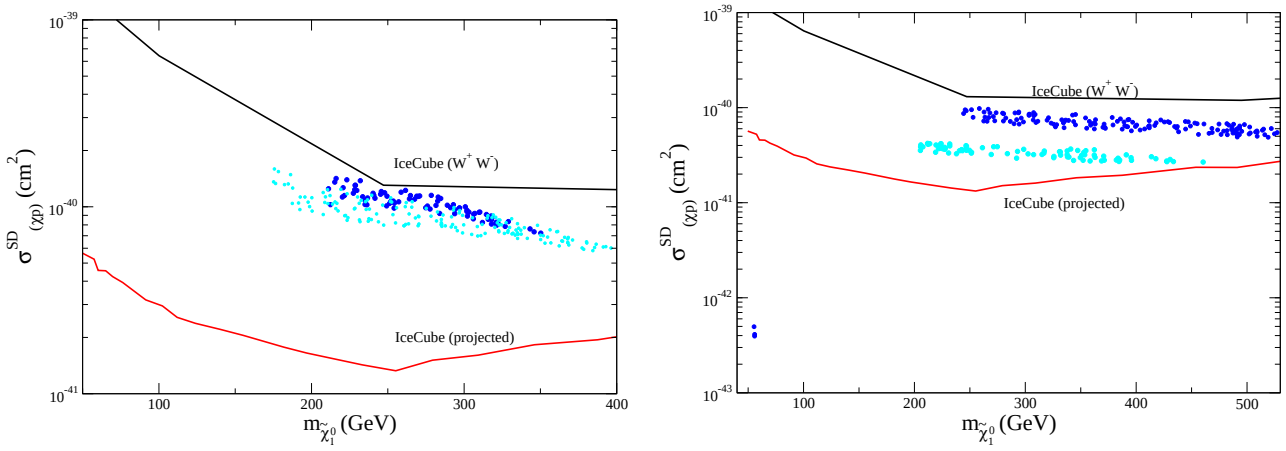
At the same time, both SI and SD cross-sections are important for the capture of DM particles within the Sun [70, 71]. Suitable models are used to relate the capture cross-section to SI and SD type of DM-nuclear cross-sections. Thus, a measurement of muon flux effectively sets limits on both SI and SD cross-sections [27, 71]. Refs. [72–74] may be seen for further details of setting the above limits and the associated degree of model dependence.

8.1 LHLRS and LMLRS

Figs. 9(a) and 9(b) show the results of scanning the aforesaid pMSSM parameter space in scatter plots of $\sigma_{p\chi}^{SD}$ vs $m_{\widetilde{\chi}_1^0}$ in the LHLRS and LMLRS models corresponding to Fig. 1 and Fig. 2 respectively. Blue and cyan points all of which satisfy the relic density, the collider limits and the $(g-2)_\mu$ data (up to the level of 3σ for low and 2σ for high $\tan\beta$) correspond to $\tan\beta = 6$ and 30 respectively in each of the figures. Limits derived from the present as well as future reach of the IceCube experiment [39, 40] are shown in black and red lines respectively. The *higgsino models* are more sensitive to the current IceCube data than the *mixed models*, as can be seen from the figures. Clearly, the final IceCube reach will exhaust the parameter space while most of the scatter points in general lie at most within an order of magnitude below the presently derived bound from the same experiment. Some points for the low $\tan\beta$ scenario in the *higgsino model* are tantalizingly close to the present limit. However, the surviving points from the Higgs resonance region for Fig. 9(b) lie way below the reach of even the final IceCube measurement.

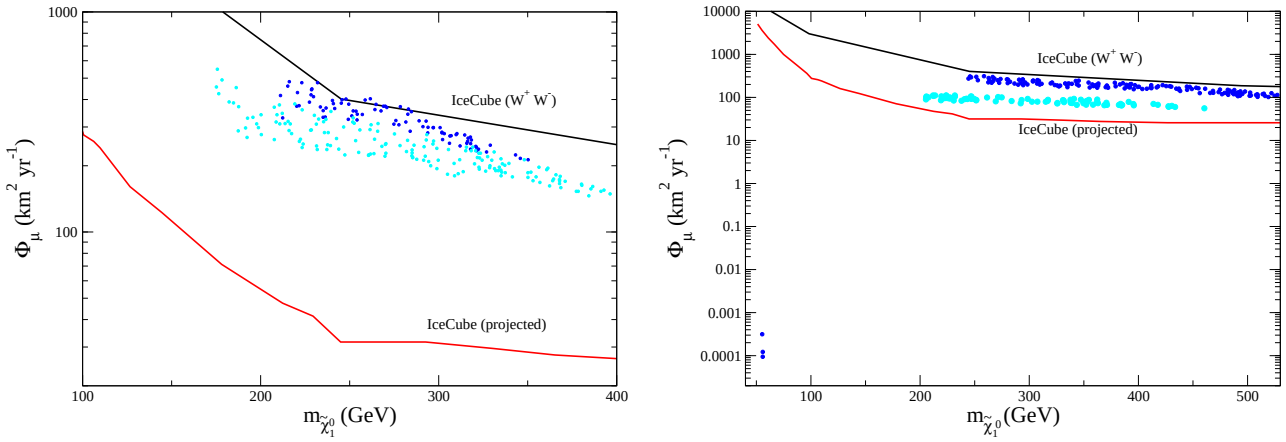
Fig. 10(a) and Fig. 10(b) show the results of muon flux Φ_μ in relation to $m_{\widetilde{\chi}_1^0}$ in the LHLRS and LMLRS models corresponding to Fig. 1 and Fig. 2 respectively. Blue and cyan points, all of which satisfy the major constraints, correspond to $\tan\beta = 6$ and 30 respectively in each of the figures. Limits on the muon flux from the present IceCube data and its future reach are shown in black and red lines respectively.

The scatter points in general lie within an order of magnitude below the presently derived bound from the IceCube. There are some points in the low $\tan\beta$ case for the *higgsino model* which lie very close to the current data. Clearly, the final IceCube reach will fully explore the parameter space, except the Higgs resonance region in Fig. 10(b), which is beyond the reach of even the future



(a) (b)

Figure 9: Plot of spin-dependent direct detection cross-section $\sigma^{SD}_{p\chi}$ vs the mass of the LSP for two cases namely (a) LHLRS : when $\widetilde{\chi}^{\pm}_1$ is principally a charged higgsino or (b) LMLRS : when $\widetilde{\chi}^{\pm}_1$ is an appreciable mixture of a charged higgsino and wino. Only the points that satisfy the relic density limits, the collider bounds and the $(g-2)_\mu$ data (up to a maximum of 3σ level for low and 2σ for high $\tan\beta$) are shown. Blue and cyan points correspond to $\tan\beta = 6$ and 30 respectively in each



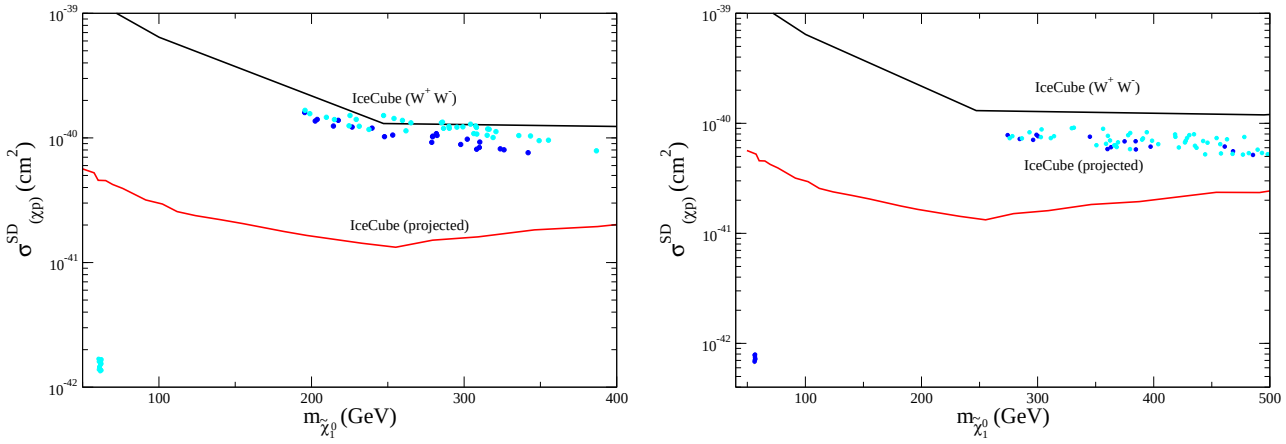
(a) (b)

Figure 10: Plot of muon-flux Φ_μ vs $m_{\widetilde{\chi}^0_1}$ for two cases : the (a) LHLRS and (b) LMLRS scenarios. Only the points that satisfy the relic density limits, the collider bounds and the $(g-2)_\mu$ data (up to 3σ level for low and 2σ level for high $\tan\beta$) are shown. Blue and cyan points correspond to $\tan\beta = 6$ and 30 respectively in each of the figures. The present and future IceCube limits are shown in black and red lines respectively.

IceCube measurement. There is a high degree of correlation between $\sigma_{p\chi}^{SD}$ and Φ_μ for a neutralino with a significant amount of higgsino mixing.

8.2 LHLS and LMLS

We compute the $\sigma_{p\chi}^{SD}$ and Φ_μ in Fig. 11 and Fig. 12 for $\tan\beta =$ 6 and 30 in the LHLS and LMLS scenarios corresponding to the analyses of Fig. 3 and Fig. 4 respectively. The results show that the valid parameter space may be effectively probed in the future IceCube measurements. However, even the future IceCube reach can not probe the Higgs resonance regions in these models since the corresponding $\sigma_{p\chi}^{SD}$ and Φ_μ values are too small.

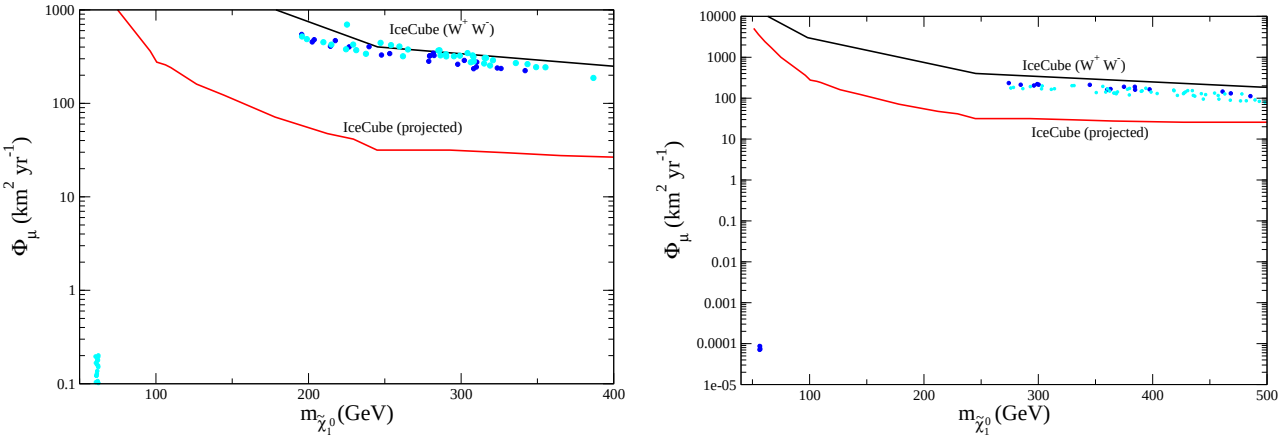


(a) (b)

Figure 11: Plot of spin-dependent direct detection cross-section vs the LSP mass for the two cases : the LHLS (a) and LMLS (b) scenarios. Colours and conventions are the same as in Fig. 9.

8.3 LHHS

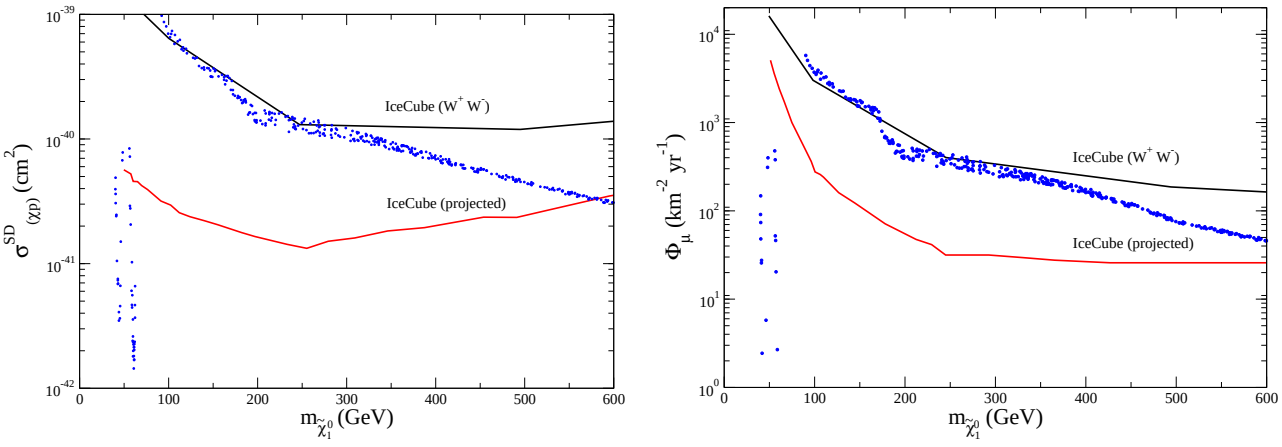
Considering the LHHS scenario associated with Fig. 5 we compute $\sigma_{p\chi}^{SD}$ and Φ_μ in Fig. 13(a) and Fig. 13(b) with $\tan\beta = 30$ for a higgsino dominated $\widetilde{\chi}_1^\pm$. Only relic density and collider satisfied points along with the $(g-2)_\mu$ constraint applied up to the level of 3σ are shown. The present and future IceCube limits are shown in black and red lines respectively. Future IceCube experiment can fully probe the allowed parameter points. However, the h-resonance region remains beyond the



(a) (b)

Figure 12: Plot of muon-flux Φ_μ vs the mass of the LSP for two cases namely the LHLS (a) and LMLS (b) scenarios. Colours and conventions are the same as in Fig. 10.

reach of even the future IceCube bounds.



(a) (b)

Figure 13: Plot of SD direct detection cross-section and muon-flux Φ_μ vs the mass of the LSP for the LHHS scenario with $\tan\beta = 30$ for a higgsino dominated $\widetilde{\chi}_1^\pm$. Only the points satisfying the relic density limits, collider constraints and the $(g-2)_\mu$ constraint applied up to the level of 3σ are shown. The present and future IceCube limits are shown in black and red lines respectively.

9 New constraints on $m_{\widetilde{g}}$ and future search prospects

In this section we consider a scenario where the gluinos, in addition to the EW sparticles, are relatively light. We choose several BPs from the LHLRS (Figs. 1(a) and 1(b)), LHLS (Fig. 3(b)) and LHHS (Fig. 5) models. Each BP captures the essential features of the corresponding model. We then compute the new $m_{\widetilde{g}}$ limits in each case using the ATLAS data for dedicated squark-gluino searches. The published data [4–8] are based on a series of conference reports [75–78]. There are a few differences between the published results and the earlier analyses so far as the details are concerned. However, there is no qualitative difference among the two sets of exclusion contours. Our analysis is based on Refs. [75–78]. This exercise also enables us to anticipate the probable signatures of different scenarios at future colliders. The characteristics of each BP are briefly described in the following lines. The underlying sparticle spectra and the relevant BRs are presented in Tables. 5-7. We like to mention that for BP2, BP4 and BP6 we consider tilted scenarios with the slepton masses driven closer to $m_{\widetilde{\chi}_1^\pm}$. As already discussed in Secs. 4.1 and 4.2, constraints from slepton searches are weakened for tilted scenarios. This allows the above-mentioned BPs which represent the Higgs resonance regions in the corresponding figures to become acceptable parameter points.

The point BP1 (BP2) is from the upper (lower) branch of the two regions satisfying the WMAP/PLANCK data in the LHLRS model (see Fig. 1(a)). From the BRs for BP1 in Table 6 and 7, it follows that in spite of the suppressed couplings of higgsino-dominated $\widetilde{\chi}_1^\pm$, $\widetilde{\chi}_2^0$ and $\widetilde{\chi}_3^0$ with appropriate fermion -sfermion pairs of the first two generations, only the trilepton signal is potentially viable for the LHC Run-II. Moreover, the BR of the invisible mode $\widetilde{\chi}_2^0 \to \nu\widetilde{\nu}$ is quite large in this case. This is a generic feature of the branch under consideration. Thus, $e^+e^- \to \not{E}_T$ events are enhanced by $\widetilde{\chi}_1^0\widetilde{\chi}_1^0$, $\widetilde{\chi}_2^0\widetilde{\chi}_2^0$ and $\nu\widetilde{\nu}$ final states [79]. Such events can be searched for at the future e^+e^- colliders using the single photon tag from initial state radiation [80]. In contrast, the invisible decays of $\widetilde{\chi}_2^0$ are rather suppressed in all other *higgsino models* studied in this paper.

BP2 is consistent with the slepton search data with a tilted slepton mass (see the discussions on the LWLRS$_{\widetilde{\chi}_1^\pm}$ and LHLRS$_{\widetilde{\chi}_1^\pm}$ models in Secs. 4.1 and 4.2). Here both $\widetilde{\chi}_2^0$ and $\widetilde{\chi}_3^0$ decay into $Z\widetilde{\chi}_1^0$ and $h\widetilde{\chi}_1^0$ while $\widetilde{\chi}_1^\pm$ decay into $W^\pm\widetilde{\chi}_1^0$ modes with large BRs. Thus, the $Wh\widetilde{\chi}_1^0$ signal will strongly compete with the reduced trilepton channel during the next phase of the LHC experiments. It may be noted that the current LHC constraints on the former signal in the *wino models* [16] are rather weak, even if the underlying decays are assumed to occur with 100% BR. It is also worth recalling

	BP1	BP2	BP3	BP4	BP5	BP6	BP7
Taken from	1a	1a (Tilted)	1b	1b (Tilted)	3b	3b (Tilted)	–
M_1	256	59.5	202	62	227	62	60
M_2	573	1000	522	1000	541	960	541
μ	286	500	261	500	270	480	271
$m_{\widetilde{\chi}_1^0}$	229	57	187	61	208	60	58
$m_{\widetilde{\chi}_1^\pm}$	281	501	258	503	269	483	268
$m_{\widetilde{\chi}_2^0}$	295	503	269	503	282	483	270
$m_{\widetilde{\chi}_3^0}$	303	510	272	511	282	490	282
$M^D_{\widetilde{(e,\mu)}_L}$	266	394	232	395	249	380	473
$M^D_{\widetilde{(e,\mu)}_R}$	265	394	232	395	2000	2000	473
$m_{\widetilde{\tau}_1}$	260	387	199	360	249	380	457
$M^D_{\widetilde{\nu}}$	255	386	219	388	236	372	466
$\Omega_{\widetilde{\chi}} h^2$	0.09	0.11	0.1	0.13	0.09	0.12	0.09
$\sigma_{SI}(pb)$ $\times 10^{-9}$	15	0.13	5.4	0.03	7.5	0.03	0.2
$a_\mu^{\rm SUSY}$ $\times 10^{-10}$	5.2	1.8	34	9.6	29	9.2	17

Table 5: The sparticle spectra corresponding to different BPs chosen from Fig. 1 and 3. All masses are given in GeV. Only the closest figures are referred with the tilted scenarios, where the figures themselves represent regular scenarios with slepton masses at the midway between the masses of the LSP and $\widetilde{\chi}_1^\pm$.

that this signal, in fact, does not look interesting in all the *wino models* except the LWHS model.

The point BP3 (BP4), consistent with all the major constraints, is taken from the upper (lower) branch of the region allowed by the WMAP/PLANCK data of Fig. 1(b). The scenario represented by BP3 has a light $\widetilde{\tau}_1$. As a result, $\widetilde{\chi}_1^\pm$ - $\widetilde{\chi}_2^0$ pairs dominantly decay into final states involving multiple τs. Thus, searches with improved τ-tagging may reveal this signature [59]. However, a small but non-negligible trilepton signal can not be ruled out *a priori*. Thus, final states involving all of the three generations of leptons in different proportions, especially at an e^+e^- collider, may be a hallmark of this model.

Decay Modes	BP1	BP2	BP3	BP4	BP5	BP6	BP7
$\widetilde{g} \to \widetilde{\chi}_1^0 t\bar{t}$	6.6	7	3.5	6	4	5.4	2.6
$\to \widetilde{\chi}_2^0 t\bar{t}$	17	18	12	14	14	14	14
$\to \widetilde{\chi}_3^0 t\bar{t}$	13	16	14	12	12	13	14
$\to \widetilde{\chi}_4^0 t\bar{t}$	1.6	-	1.7	-	1.5	-	1.5
$\to \widetilde{\chi}_1^0 b\bar{b}$	1.2	3	2.3	3	3	2.4	1.4
$\to \widetilde{\chi}_2^0 b\bar{b}$	-	0.4	4.4	6.5	5	6.5	5.4
$\to \widetilde{\chi}_3^0 b\bar{b}$	0.5	0.3	5	6.3	4	6.2	5
$\to \widetilde{\chi}_4^0 b\bar{b}$	2.7	0.2	2.6	-	2.5	-	2.4
$\to \widetilde{\chi}_1^\pm t\bar{b}$	44	52	42	50	44	50	44
$\to \widetilde{\chi}_2^\pm t\bar{b}$	9.6	-	9.4	-	9.0	-	8
$\widetilde{\chi}_1^\pm \to \widetilde{\nu}_\tau \tau$	32	3	37	18	69	21.4	-
$\to \widetilde{\tau}_1 \nu_\tau$	8	1.5	46	15	1.4	0.4	-
$\to \widetilde{\tau}_2 \nu_\tau$	-	-	-	2.6	-	-	-
$\to \widetilde{\nu}_l l$	53	4	15	2.6	28	3.6	-
$\to \widetilde{l}_L \nu_l$	6.8	1.2	1.8	0.6	2.6	0.8	-
$\to W^\pm \widetilde{\chi}_1^0$	-	90	-	61	-	74	100

Table 6: Dominant decay modes and BRs of gluino and chargino for different BPs taken from Fig. 1 and Fig. 3.

BP4 similarly represents the generic features of the Higgs resonance region of Fig. 1(b). As in the previous case, final states with varieties of leptons belonging to all of the three generations is a feature of this scenario. However, the signal $Wh\widetilde{\chi}_1^0$, if kinematically allowed, also looks promising for the LHC Run-II. Since the probability of τ-rich final states is still sizable, observing both $\tau h\widetilde{\chi}_1^0$ and $Wh\widetilde{\chi}_1^0$ could be a smoking-gun signal. The former signature, though challenging at a hadron collider, is expected to be rather straightforward at an e^+e^- machine.

BP5 (BP6) captures the generic features of the upper (lower) branch of the region allowed by the WMAP/PLANCK data of Fig. 3(b) quite well. Both the points are consistent with all the major constraints provided the slepton mass is tilted towards $m_{\widetilde{\chi}_1^\pm}$. BP5 also represents a scenario where all three generations of leptons may appear in the final state in different combinations, although a clear τ-dominance is noticeable since the electroweakinos are higgsino-dominated. However, for

Decay Modes	BP1	BP2	BP3	BP4	BP5	BP6	BP7
$\widetilde{\chi}_2^0 \to \widetilde{l}_L^{\pm} l^{\mp}$	2	4	17.6	2.64	0.6	3.6	-
$\to \widetilde{\nu}\bar{\nu}$	57.6	1.2	0.5	0.8	18	1.2	-
$\to \widetilde{l}_R^{\pm} l^{\mp}$	10	1.6	22	0.8		-	-
$\to \widetilde{\tau}_1^{\pm} \tau^{\mp}$	7.4	3	58	28	82	20	-
$\to \widetilde{\tau}_2^{\pm} \tau^{\mp}$	22	1.4	1	6	-		-
$\to \widetilde{\chi}_1^0 h$	-	65	-	38	-	48	62
$\to \widetilde{\chi}_1^0 Z$	-	22	-	22	-	28	38
$\widetilde{\chi}_3^0 \to \widetilde{l}_L^{\pm} l^{\mp}$	24	-		-	48		-
$\to \widetilde{\nu}\bar{\nu}$	4.8	0.6	8.4	0.96	6	1.2	-
$\to \widetilde{l}_R^{\pm} l^{\mp}$	40	0.4	1.6	0.4		-	-
$\to \widetilde{\tau}_1^{\pm} \tau^{\mp}$	19.2	-	86	22	46	20	-
$\to \widetilde{\tau}_2^{\pm} \tau^{\mp}$	12.8	1.4	4	10	-	-	-
$\to \widetilde{\chi}_1^0 h$		22	-	22	-	26	20
$\to \widetilde{\chi}_1^0 Z$	-	74	-	43	-	53	80

Table 7: Dominant decay modes and BRs of $\widetilde{\chi}_2^0$ and $\widetilde{\chi}_3^0$ for different BPs taken from Fig. 1 and Fig. 3.

BP6 the τ-dominance is relatively mild. The $Wh\widetilde{\chi}_1^0$ signal, as and when sufficient luminosity accumulates, appears to be an attractive option.

BP7 is from Fig. 5 and is consistent with all the major constraints. Here both the trilepton and the $Wh\widetilde{\chi}_1^0$ events are expected to show up. However, it follows from Table 6 and 7 that the relative rate of the later class of events are expected to be larger. As in the LWHS model, the LHHS model promises signatures other than the conventional trileptons from chargino-neutralino production.

The gluino decay BRs for different scenarios are also presented in Table 6. Since $\widetilde{\chi}_1^{\pm}$, $\widetilde{\chi}_2^0$ and $\widetilde{\chi}_3^0$ are higgsino-dominated, the final states with third generation of quarks overwhelm those containing leptons or light quark jets. Thus, it is expected that the search channels with tagged b-jets would yield the most stringent mass bounds on $m_{\widetilde{g}}$ from current data. It also follows that these are the best channels for gluino search in the *higgsino model* during the LHC Run-II.

Before we compute the revised gluino mass limits in the *higgsino models*, we summarise the

ATLAS SUSY searches sensitive to gluino pair production. After analysing the LHC Run-I ($\mathcal{L} \sim$ 20 fb^{-1}) data, the ATLAS collaboration interpreted the results in the n-leptons + m-jets (with or without b tagging) + $\not{E}_T$ channel with different integral values of n and m for various simplified models [75–78]. For the inclusive jets + $0l$ + $\not{E}_T$ channel, depending on jet multiplicities, they defined five inclusive analyses channels (labelled as A to E) [75]. The selection criteria used for 11 signal regions (SRs) are summarised in Table 1 of Ref. [75]. In the absence of any significant excess, an upper limit on the number of events (N_{BSM}) from any Beyond the Standard Model (BSM) scenario was presented for various signal regions. The most effective signal regions for our analysis and the corresponding upper limits on N_{BSM} for $\mathcal{L} = 20.3$ fb^{-1} are presented in Table 8.

Channel	Most effective signal Regions	Observed upper limits on N_{BSM} (95 % CL)
Jets $+0l + \not{E}_T$ [75]	SRC-Medium	81.2
	SRD	15.5
	SRE-Medium	28.6
	SRE-Tight	8.3
Jets $+1l + \not{E}_T$ [76]	Inclusive 6-jet(e)	4.6
	Inclusive 6-jet(μ)	3.0
Jets+2$SSl - 3l + \not{E}_T$ [77]	SR3b	3.9
Jets (3b) $+0 - 1l + \not{E}_T$ [78]	SR-1l-6j-B	3.0

Table 8: The most effective signal regions for our analysis and the corresponding upper limits on N_{BSM} at 95 % CL with $\mathcal{L} = 20.3$ fb^{-1} in the jets + $0l$ + $\not{E}_T$ channel [75], jets + $1l$ + $\not{E}_T$ channel [76], jets+2$SSl - 3l + \not{E}_T$ channel [77] and $0l$ +jets (3b) + $\not{E}_T$ [78] channel.

We adopt the analysis of "hard single-lepton" ($n = 1$) from Ref. [76]. In this channel, the ATLAS collaboration defined six inclusive and six binned signal regions treating electrons and muons independently. Details of the signal regions are summarised in Table 4 of Ref. [76]. For our case, the most effective signal regions are inclusive 6-jet (electron) and 6-jet (muon) (for the upper limits on N_{BSM} in these two channels, see Table 8).

For the same sign (SS) dilepton analysis, the ATLAS collaboration considered either two iso-

lated leptons (e or μ) with the same electric charge, or at least three isolated leptons ($3l$) [77]. The *SR3b* signal region yields the best limits for the *higgsino models*. In this signal region, SS or $3l$ events are chosen with at least five jets and at least three b-jets. Corresponding upper limit on N_{BSM} for $\mathcal{L} = 20.3$ fb^{-1} is 3.9 [77]. Details of the selection criteria for the other signal regions are presented in Table 1 of [77].

Next, we will briefly discuss the most important channel - jets (at least 3 b-jets) + 0-1l ($l = e, \mu$) + $\not{E}_T$ [78] which gives the most stringent bounds on $m_{\widetilde{g}}$ in the *higgsino models*. Selection criteria for the 9 signal regions are listed in Tables 1 and 2 of Ref. [78] and upper limits on N_{BSM} at 95 % confidence level (CL) are presented in Table 5 of Ref. [78]. The most effective signal region is $SR-1l-6j-C$[16], characterized by large $\not{E}_T$ and at least six jets which includes at least three b-tagged jets.

For electron, muon and jet identification, lepton-lepton isolation, lepton-jet isolation etc., we follow the ATLAS prescription as described in Refs. [75–78]. For b-tagging, we use the P_T dependent b-tagging efficiencies presented by ATLAS collaboration in Ref. [81]. After reconstruction of objects, we adopt all the signal regions defined by different selection criteria, introduced in Refs. [75–78]. For validation purpose, we also match the number of events and efficiencies of different cuts used for different signal regions in Refs. [75–78] with the ATLAS results.

Using PYTHIA (v6.428) [36] we generate the signal events in various channels from gluino pair production for the chosen BPs. For the NLO $\widetilde{g}\widetilde{g}$ pair production cross-section calculation we use PROSPINO 2.1 [42] with CTEQ6.6M PDF [82]. By comparing the simulated number of events with the corresponding upper limits on N_{BSM} in the appropriate signal region, we calculate the new limits on $m_{\widetilde{g}}$ for different scenarios represented by BP1 - BP7.

The revised limits on $m_{\widetilde{g}}$ in different *higgsino models* are presented in Table 9. As expected, the strongest limits come from search channels involving tagged b-jets. The limits are practically independent of the choice of the slepton masses. It may be recalled that in the *wino model* the best limits come from the jets+$1l$+$\not{E}_T$ channel. This table also illustrates the importance of multichannel search for the *higgsino model*. The size of jets+$0l$ + $\not{E}_T$ signal can potentially distinguish some of the *higgsino models* from the others. However, our results are based on the generic strategies for squark-gluino searches devised by the ATLAS collaboration using tagged b-jets. In the LHC Run-

[16] signal regions are classified as $A/B/C$ depending on $\not{E}_T$ and m_{eff}.

Points	Limit on $m_{\widetilde{g}}$ (GeV)			
	jets $+0l + \not{E}_T$ [75]	jets $+1l + \not{E}_T$ [76]	jets $+2l + \not{E}_T$ [77]	$0l$ +jets (3b) $+ \not{E}_T$ [78]
BP1	675	1125	1250	1340
BP2	1080	1175	1135	1360
BP3	815	1100	1180	1320
BP4	1050	1160	1135	1345
BP5	770	1105	1210	1330
BP6	1075	1160	1135	1345
BP7	980	1130	1135	1325

Table 9: Limits on $m_{\widetilde{g}}$ for different BPs using the ATLAS jets + $0l$ + $\not{E}_T$ data [75], jets + $1l$ + $\not{E}_T$ data [76], jets $+2l + \not{E}_T$ (SSD) data [77] and $0l$ +jets(3b) + $\not{E}_T$ [78] data.

II, more dedicated searches, e.g., the detection of a Higgs boson in a gluino decay cascade may provide more definite information on the underlying *higgsino model*.

10 Conclusion

The focus of this paper is on the phenomenology of the *higgsino* and the *mixed models* of the electroweakinos and to compare and contrast them with that of the corresponding *wino models* studied in Ref. [24]. In this concluding section we summarize our main results in the light of the three major constraints (see Table 10).

To give the readers some feelings for the numerical values of the revised LHC mass limits we note that in the LHLRS (for low $\tan\beta$) and LHLS (for both values of $\tan\beta$) models the lower bounds on $m_{\widetilde{\chi}_1^\pm}$ are 380 GeV and 360 GeV respectively. These bounds are significantly weaker than the similar bounds in the corresponding *wino models* which have the ballpark values of ~ 600 GeV. It is interesting to note that the entire exclusion contour in the LHLRS model with high $\tan\beta$ is superseded by the theoretical constraints. However, for small LSP masses, the bounds from the slepton searches translate into stronger bounds: $m_{\widetilde{\chi}_1^\pm} \geq 650$ GeV (LHLRS) and 600 GeV (LHLS). As discussed in detail in the text these bounds get weaker in the tilted LHLRS$_{\widetilde{\chi}_1^\pm}$ and LHLS$_{\widetilde{\chi}_1^\pm}$

Model	Trilepton Constraint	Processes Leading to Correct Relic density	The $(g-2)_\mu$ Constraint Satisfied at
LHLRS	Degraded w.r.t. the LWLRS case	$\widetilde{\chi}_1^0\widetilde{\chi}_1^0 \to W^+W^-, t\bar{t}, ZZ, Zh$ Z/h resonance annihilation $\widetilde{\tau}_1$ coannihilation (only for high $\tan\beta$)	(a) 3σ (low $\tan\beta$) (b) $\leq 2\sigma$ (high $\tan\beta$)
LHLS	Degraded w.r.t. the LWLS case	$\widetilde{\chi}_1^0\widetilde{\chi}_1^0 \to W^+W^-, t\bar{t}, ZZ$ Z/h resonance annihilation	Same as above
LHHS	Degraded w.r.t. the LWHS case.	$\widetilde{\chi}_1^0\widetilde{\chi}_1^0 \to W^+W^-, ZZ, t\bar{t}$ Z/h resonance annihilation	$\leq 2\sigma$ for high $\tan\beta$
LMLRS	Degraded w.r.t. the LWLRS case but stronger than the LHLRS model.	$\widetilde{\chi}_1^0\widetilde{\chi}_1^0 \to W^+W^-, t\bar{t}$ Z/h resonance annihilation $\widetilde{\tau}_1$ coannihilation (only for high $\tan\beta$)	(a) 3σ (low $\tan\beta$) (b) $\leq 2\sigma$ (high $\tan\beta$)
LMLS	Degraded w.r.t. the LWLS case. but stronger than the LHLS model	$\widetilde{\chi}_1^0\widetilde{\chi}_1^0 \to W^+W^-, t\bar{t}, ZZ$ Z/h resonance annihilation	Same as above

Table 10: Summary of the impact of the three major constraints on the models analyzed in this work. Here, LWLS corresponds to the Light Wino and Light Left Sleptons model. Similarly, LWLRS refers to the Light Wino and Light Left and Right Sleptons and LWHS corresponds to the Light Wino and Heavy Sleptons scenarios respectively. These *wino models* were discussed in detail in Ref. [24].

models yielding $m_{\widetilde{\chi}_1^\pm} \geq 450$ GeV (LHLRS) and 410 (LHLS) GeV. For higher LSP masses both the bounds obtained directly from the trilepton searches and those deduced from the constraints in the slepton sector become relaxed and eventually disappear for certain LSP masses which for each model can easily be read off from the figures concerned. In the LHHS model the bound is $m_{\widetilde{\chi}_1^\pm} \geq$ 175 GeV for negligible LSP masses. This is rather weak even in comparison with the corresponding limit in the LWHS model which is the most relaxed limit among the *wino models*. We have also considered the LHC constraints in the *mixed models*. As expected, the LHC limits lie in between the corresponding ones in the *wino* and the *higgsino models*. However, no qualitatively new feature emerges from this analysis.

In all models considered in this paper and in Ref [24] with low $\tan\beta$ the predictions for $(g-2)_\mu$

are consistent with the data only at the level of 3σ after imposing the LHC constraints. The constraint can be more effective only in high $\tan\beta$ scenarios.

In the parameter spaces of the *higgsino* and the *mixed models* there are two distinct branches allowed by the WMAP/PLANCK constraints, as in the *wino models*. In the upper branches the LSP pair annihilations into various channels turn out to be the dominant DM relic density producing mechanism as illustrated in Table 10. Only in the LHLRS and the LMLRS models with large $\tan\beta$, the LSP-stau coannihilation is important. In contrast, the upper branches in the *wino models* are dominated by different coannihilation processes.

In the lower branches of the *higgsino* and the *mixed models* analyzed in this work, the DM production is mainly due to LSP pair annihilation via the h-resonance. The APSs are larger in models with tilted slepton masses for reasons explained in the text. In contrast, this mechanism is generically under pressure in the *wino models* with heavy sleptons either due to the above tension with the $(g-2)_\mu$ constraint or due to the LHC constraints or both.

The inclusion of the WMAP/PLANCK and the $(g-2)_\mu$ constraints in our analysis severely restricts the APSs by imposing both upper and lower mass bounds in most of the models studied here. At high $\tan\beta$, most of the *wino*, *mixed* and the *higgsino models* have narrow APSs surviving all the major constraints. We now summarize our main findings regarding the prospects of having novel signatures at the LHC Run-II and at the ILC.

In the *higgsino models* $\widetilde{\chi}_2^0$ or $\widetilde{\chi}_3^0$ decaying into $Zh\widetilde{\chi}_1^0$ with large BR are rather common (see the examples in Table 7). They occur even if the sleptons are lighter than the electroweakinos. In contrast, these decays occur with large BRs in the *wino models* with heavy sleptons provided the DM constraints are relaxed. The discovery of light sleptons together with the observation of the $Wh\not{E}_T$ events due to chargino-neutralino production during the LHC Run-II could be the hallmark of the *higgsino models*. If we focus on this signal in parameter spaces consistent with the $(g-2)_\mu$ and the DM relic density constraints, then only zones with high $\tan\beta$ and DM relic density production via LSP pair annihilation into the h-resonance are acceptable. On the other hand this DM producing mechanism is generically disfavoured in the *wino models* with high $\tan\beta$ as noted earlier.

In some regions of the APSs, especially in the upper branches of the regions allowed by the WMAP/PLANCK data in the $m_{\widetilde{\chi}_1^\pm} - m_{\widetilde{\chi}_1^0}$ plane, the conventional trilepton channel appears to be

the best bet in many models considered in this paper and in Ref. [24]. With improved τ-tagging efficiencies, the final states with multiple τ's as analysed in Ref. [59] for models with high $\tan\beta$ may provide alternative/complementary search channels during the LHC Run-II. Several novel signatures which could be relevant at the ILC have also been discussed in Sec. 9. In particular, the comparison of the constraints obtained in this paper and the ones in Ref. [24] clearly indicates that if the ILC indeed operates at around 500 GeV during its first run as planned, then the electroweakinos in the *higgsino model* have larger probabilities of being within its striking range (see, for e.g., Fig. 5).

Assuming the gluinos to be light in addition to the electroweak sparticles while all squarks are heavy, we have revisited the gluino mass limits in Sec. 9 using the ATLAS data. As in the *wino model*, this analysis emphasizes the importance of multichannel searches. It follows that the conventional jets + 0 l + $\not\!\!E_T$ signal has the poorest sensitivity in a wide variety of the *higgsino models* (see the results in Table 9 for different BPs in Sec. 9), whereas jets + 1l or 2l + $\not\!\!E_T$ signal has a better sensitivity. The best channel for probing the *higgsino models* involves multiple tagged b-jets. The gluino mass limits are stronger in general than the ones obtained in the corresponding *wino models*. This observation may help to formulate the future strategies for gluino searches in the context of the *higgsino models* and distinguish between the *wino* and the *higgsino models*, if a signal is seen. Moreover, one can distinguish among various *higgsino models* consistent with the major constraints by the relative rates of jets + 0 l + $\not\!\!E_T$ and jets (3b)+ 0 l + $\not\!\!E_T$ events (see Table 8).

We next summarize the prospects of direct and indirect detection of DM in the context of the *higgsino* models. There is a significant bino-higgsino mixing in the LSP in the *higgsino models* especially in the portions of the parameter spaces consistent with the DM relic density constraint and characterized by relatively small $m_{\widetilde{\chi}_1^\pm} - m_{\widetilde{\chi}_1^0}$. The spin-independent direct detection cross-section $\sigma^{\rm SI}_{\tilde{\chi}p}$ is larger in all such cases compared to the corresponding *wino models*. Although the cross-sections exceed the LUX limits in most of the cases, they stay within an order of magnitude of the same limits. However, the cross-section for the points from the Higgs resonance region allowed by the major constraints (e.g. in Figs. 6(b), 7 and 8) lie well below the LUX limit. All the models can be probed by the future XENON1T experiment irrespective of the degree of uncertainties in $\sigma^{\rm SI}_{\tilde{\chi}p}$.

The spin-dependent cross-section $\sigma^{\rm SD}_{\tilde{\chi}p}$ and muon flux values for the neutrino signals in the

higgsino models are enhanced compared to their *wino* model counterparts. Most of the points in almost all the scenarios are allowed by the present IceCube data. In some cases the situation seems very interesting since the values of $\sigma_{\tilde{\chi}p}^{\rm SD}$ and muon flux lie very close to the present experimental bound (see e.g. Figs. 9(a), 10(a), 11(a), 12(a) and 13). All the other cases would decisively be probed by the future IceCube searches. For the points representing the h-resonance region in Figs. 9(b), 10(b), 11, 12 and 13 the values of these observables are too small to be detected even by the future IceCube reach.

Acknowledgments : MC would like to thank Council of Scientific and Industrial Research, Government of India for financial support. The work of AC was partially supported by funding available from the Department of Atomic Energy, Government of India for the Regional Centre for Accelerator-based Particle Physics (RECAPP), Harish-Chandra Research Institute. AD acknowledges the award of a Senior Scientist position by the Indian National Science Academy.

References

[1] For reviews on supersymmetry, see, *e.g.*, H. P. Nilles, Phys. Rep. **110**, 1 (1984); J. D. Lykken, [arXiv:hep-th/9612114]; J. Wess and J. Bagger, *Supersymmetry and Supergravity*, 2nd ed., (Princeton, 1991).

[2] H. E. Haber and G. Kane, Phys. Rep. **117**, 75 (1985); S. P. Martin, [arXiv:hep-ph/9709356]; D. J. H. Chung *et al.*, Phys. Rept. **407**, 1 (2005) [arXiv:hep-ph/0312378];

[3] M. Drees, P. Roy and R. M. Godbole, *Theory and Phenomenology of Sparticles*, (World Scientific, Singapore, 2005); H. Baer and X. Tata, *Weak scale supersymmetry: From superfields to scattering events*, Cambridge, UK: Univ. Pr. (2006) 537 p.

[4] G. Aad *et al.* [ATLAS Collaboration], JHEP **1409**, 176 (2014) [arXiv:1405.7875].

[5] G. Aad *et al.* [ATLAS Collaboration], JHEP **1504**, 116 (2015) [arXiv:1501.03555].

[6] G. Aad *et al.* [ATLAS Collaboration], JHEP **1406**, 035 (2014) [arXiv:1404.2500].

[7] G. Aad *et al.* [ATLAS Collaboration], JHEP **1410**, 24 (2014) [arXiv:1407.0600].

[8] G. Aad *et al.* [ATLAS Collaboration], [arXiv:1503.03290].

[9] S. Chatrchyan *et al.* [CMS Collaboration], Phys. Lett. B **733**, 328 (2014) [arXiv:1311.4937]. JHEP **1401**, 163 (2014) [JHEP **1501**, 014 (2015)] [arXiv:1311.6736]; JHEP **1406**, 055 (2014) [arXiv:1402.4770]; V. Khachatryan *et al.* [CMS Collaboration], Phys. Lett. B **745**, 5 (2015) [arXiv:1412.4109]; Phys. Rev. D **91**, 052018 (2015) [arXiv:1502.00300]; JHEP **1505**, 078 (2015) [arXiv:1502.04358]; JHEP **1504**, 124 (2015) [arXiv:1502.06031];

[10] T. J. LeCompte and S. P. Martin, Phys. Rev. D **85**, 035023 (2012) [arXiv:1111.6897]; B. Bhattacherjee and K. Ghosh, [arXiv:1207.6289]; H. K. Dreiner, M. Kramer and J. Tattersall, Phys. Rev. D **87**, 035006 (2013) [arXiv:1211.4981]. B. Bhattacherjee, A. Choudhury, K. Ghosh and S. Poddar, Phys. Rev. D **89**, 037702 (2014) [arXiv:1308.1526].

[11] N. Sakai, Zeit. Phys. C 11 (1981) 153; R. K. Kaul and P. Majumdar, Nucl. Phys. B **199** (1982) 36; R. Barbieri and G. F. Giudice, Nucl. Phys. B **306** (1988) 63.

[12] K. L. Chan, U. Chattopadhyay and P. Nath, Phys. Rev. D **58**, 096004 (1998); [arXiv:hep-ph/9710473]; J. L. Feng, K. T. Matchev and T. Moroi, Phys. Rev. D **61**, 075005 (2000); Phys. Rev. Lett. **84**, 2322 (2000) [arXiv:hep-ph/9908309]; U. Chattopadhyay, A. Corsetti and P. Nath, Phys. Rev. D **68**, 035005 (2003) [arXiv:hep-ph/0303201]; S. Akula, M. Liu, P. Nath and G. Peim, Phys. Lett. B **709**, 192 (2012) [arXiv:1111.4589] J. L. Feng, Ann. Rev. Nucl. Part. Sci. 63 (2013) 351-382, [arXiv:1302.6587]; H. Baer, V. Barger, M. Padeffke-Kirkland and X. Tata, Phys. Rev. D **89** (2014) 037701, [arXiv:1311.4587]; H. Baer, V. Barger, D. Mickelson and M. Padeffke-Kirkland, [arXiv:1404.2277]; A. Mustafayev and X. Tata, [arXiv:1404.1386].

[13] G. Aad *et al.* [ATLAS Collaboration], Phys. Lett. B **716**, 1 (2012) [arXiv:1207.7214 [hep-ex]]; S. Chatrchyan *et al.* [CMS Collaboration], Phys. Lett. B **716**, 30 (2012) [arXiv:1207.7235 [hep-ex]].

[14] A. Djouadi, Phys. Rept. **459**, 1 (2008) [arXiv:hep-ph/0503173].

[15] M. Flechl [ATLAS for and CMS Collaborations], [arXiv:1503.00632].

[16] G. Aad *et al.* [ATLAS Collaboration], JHEP **1404**, 169 (2014) [arXiv:1402.7029].

[17] G. Aad *et al.* [ATLAS Collaboration], JHEP **1405**, 071 (2014) [arXiv:1403.5294].

[18] G. Aad *et al.* [ATLAS Collaboration], JHEP **1410**, 96 (2014) [arXiv:1407.0350].

[19] G. Aad *et al.* [ATLAS Collaboration], Eur. Phys. J. C **75**, 208 (2015) [arXiv:1501.07110].

[20] V. Khachatryan *et al.* [CMS Collaboration], Phys. Rev. D **90**, 092007 (2014) [arXiv:1409.3168].

[21] V. Khachatryan *et al.* [CMS Collaboration], Eur. Phys. J. C **74**, 3036 (2014) [arXiv:1405.7570].

[22] D. Ghosh, M. Guchait and D. Sengupta, Eur. Phys. J. C **72**, 2141 (2012) [arXiv:1202.4937]; K. Howe and P. Saraswat, JHEP **10**, 065 (2012) [arXiv:1208.1542]; A. Arbey, M. Battaglia and F. Mahmoudi, Eur. Phys. J. C **75**, 108 (2015) [arXiv:1212.6865]; A. Bharucha, S. Heinemeyer and F. von der Pahlen, Eur. Phys. J. C **73**, 2629 (2013) [arXiv:1307.4237]; T. Han, S. Padhi and S. Su, Phys. Rev. D **88**, 115010 (2013) [arXiv:1309.5966]; A. Papaefstathiou, K. Sakurai and M. Takeuchi, JHEP **1408**, 176 (2014) [arXiv:1404.1077]; F. Yu, Phys. Rev. D **90**, 015009 (2014) [arXiv:1404.2924].

[23] A. Choudhury and A. Datta, JHEP **09**, 119 (2013) [arXiv:1305.0928], J. Eckel, M. J. Ramsey-Musolf, W. Shepherd and S. Su, JHEP **1411**, 117 (2014) [arXiv:1408.2841], C. Han, L. Wu, J. M. Yang, M. Zhang and Y. Zhang, Phys. Rev. D **91**, 055030 (2015) [arXiv:1409.4533], C. Han, [arXiv:1409.7000].

[24] M. Chakraborti, U. Chattopadhyay, A. Choudhury, A. Datta and S. Poddar, JHEP **1407**, 019 (2014) [arXiv:1404.4841].

[25] A. Djouadi *et al.* [MSSM Working Group Collaboration], [hep-ph/9901246].

[26] C. Jungman, M. Kamionkowski and K. Griest, Phys. Rep. **267**, 195 (1996) [arXiv:hep-ph/9506380].

[27] G. Bertone, D. Hooper and J. Silk, Phys. Rept. **405**, 279 (2005) [arXiv:hep-ph/0404175];

[28] A. Lahanas, N. Mavromatos and D. Nanopoulos, Int. J. Mod. Phys. D 12, 1529 (2003) [arXiv:hep-ph/0308251]; W. L. Freedman and M. S. Turner, Rev. Mod. Phys. **75**, 1433 (2003) [arXiv:astro-ph/0308418]; L. Roszkowski, Pramana **62**, 389 (2004) [arXiv:hep-ph/0404052]; K. Olive, [arXiv:astro-ph/0503065]; H. Baer and X. Tata, [arXiv:0805.1905], in *Physics at the Large Hadron Collider*, Indian National Science Academy, A Platinum Jubilee Special Issue

(Eds. A. Datta, B. Mukhopadhyaya and A. Raychaudhuri; Springer, 2009). M. Drees and G. Gerbier, [arXiv:1204.2373]; S. Arrenberg *et al.*, [arXiv:1310.8621].

[29] G. Hinshaw *et al.*, (WMAP Collaboration), [arXiv:1212.5226].

[30] P. A. R. Ade, *et al.*, [Planck Collaboration], [arXiv:1303.5076].

[31] G. Belanger, F. Boudjema, A. Cottrant, R. M. Godbole and A. Semenov, Phys. Lett. B **519**, 93 (2001) [arXiv:hep-ph/0106275]; U. Chattopadhyay, D. Das, P. Konar and D. P. Roy, Phys. Rev. D **75**, 073014 (2007) [arXiv:hep-ph/0610077]; U. Chattopadhyay, D. Das, A. Datta and S. Poddar, Phys. Rev. D **76**, 055008 (2007) [arXiv:0705.0921]; R. M. Godbole, M. Guchait and D. P. Roy, Phys. Rev. D **79**, 095015 (2009) [arXiv:0807.2390]; U. Chattopadhyay and D. Das, Phys. Rev. D **79**, 035007 (2009) [arXiv:0809.4065]; U. Chattopadhyay, D. Das and D. P. Roy, Phys. Rev. D **79**, 095013 (2009) [arXiv:0902.4568]; D. Feldman, Z. Liu and P. Nath, Phys. Rev. D **80**, 015007 (2009) [arXiv:0905.1148]; D. Feldman, Z. Liu, P. Nath and B. D. Nelson, Phys. Rev. D **80**, 075001 (2009) [arXiv:0907.5392]; U. Chattopadhyay, D. Das, D. K. Ghosh and M. Maity, Phys. Rev. D **82**, 075013 (2010) [arXiv:1006.3045]; M. A. Ajaib, T. Li and Q. Shafi, Phys. Rev. D **85**, 055021 (2012) [arXiv:1111.4467]; A. Choudhury and A. Datta, Mod. Phys. Lett. A 27 (2012) 1250188 [arXiv:1207.1846]; S. Mohanty, S. Rao and D. P. Roy, J. High Energy Phys.11 (2012) 175 [arXiv:1208.0894]; M. Chakraborti, U. Chattopadhyay and R. M. Godbole, Phys. Rev. D **87**, no. 3, 035022 (2013) [arXiv:1211.1549 [hep-ph]]; S. Bhattacharya, S. Chakdar, K. Ghosh and S. Nandi, Phys. Rev. D **89**, 015004 (2014), [arXiv:1309.0036]; K. Harigaya, K. Kaneta and S. Matsumoto, [arXiv:1403.0715], M. Frank and S. Mondal, Phys. Rev. D **90**, no. 7, 075013 (2014) [arXiv:1408.2223]; D. Francescone, S. Akula, B. Altunkaynak and P. Nath, JHEP **1501**, 158 (2015) [arXiv:1410.4999 [hep-ph]]; L. Calibbi, J. M. Lindert, T. Ota and Y. Takanishi, JHEP **1411**, 106 (2014) [arXiv:1410.5730]; J. Bramante, P. J. Fox, A. Martin, B. Ostdiek, T. Plehn, T. Schell and M. Takeuchi, Phys. Rev. D **91**, no. 5, 054015 (2015) [arXiv:1412.4789]; F. Wang, W. Wang and J. M. Yang, JHEP **1503**, 050 (2015) [arXiv:1501.02906].

[32] S. Akula, D. Feldman, Z. Liu, P. Nath and G. Peim, Mod. Phys. Lett. A 26 (2011) 1521 [arXiv:1103.5061]; N. Bhattacharyya, A. Choudhury and A. Datta, Phys. Rev. D **83**, 115025 (2011) [arXiv:1104.0333]; N. Bhattacharyya, A. Choudhury and A. Datta, Phys. Rev. D

84, 095006 (2011) [arXiv:1107.1997]; S. Akula *et al.*, Phys. Rev. D **85**, 075001 (2012) [arXiv:1112.3645]; K. A. Olive, [arXiv:1202.2324]; D. Ghosh, M. Guchait, S. Raychaudhuri and D. Sengupta, Phys. Rev. D **86**, 055007 (2012) [arXiv:1205.2283]; P. Nath, [arXiv:1207.5501]; J. Ellis, Eur. Phys. J. C **74**, 2732 (2014) [arXiv:1312.5426].

[33] D. A. Vasquez, G. Belanger and C. Boehm, Phys. Rev. D **84**, 095015 (2011) [arXiv:1108.1338]; A. Choudhury and A. Datta, JHEP **06** (2012) 006 [arXiv:1203.4106]; A. J. Williams, C. Boehm, S. M. West and D. A. Vasquez, Phys. Rev. D **86**, 055018 (2012) [arXiv:1204.3727]; A. Arbey, M. Battaglia, A. Djouadi, F. Mahmoudi, Phys. Lett. B **720** (2013) 153, [arXiv:1211.4004]; G. Arcadi, R. Catena and P. Ullio, [arXiv:1211.5129]; C. Boehm, P. S. B. Dev, A. Mazumdar and E. Pukartas, JHEP **06** (2013) 113 [arXiv:1303.5386]; S. Scopel, N. Fornengo and A. Bottino, [arXiv:1304.5353]; J. A. Casas, J. M. Moreno, K. Rolbiecki and B. Zaldivar, [arXiv:1305.3274]; B. Bhattacherjee, M. Chakraborti, A. Chakraborty, U. Chattopadhyay, D. Das and D. K. Ghosh, Phys. Rev. D **88** (2013) 035011 [arXiv:1305.4020]; A. Fowlie, K. Kowalska, L. Roszkowski, E. M. Sessolo and Y. L. S. Tsai, Phys. Rev. D **88**, 055012 (2013) [arXiv:1306.1567]; A. Arbey, M. Battaglia and F. Mahmoudi, Phys. Rev. D **88**, 095001 (2013) [arXiv:1308.2153]; A. Pierce, N. R. Shah, K. Freese [arXiv:1309.7351]; K. Kowalska, L. Roszkowski, E. M. Sessolo and S. Trojanowski, JHEP **1404**, 166 (2014) [arXiv:1402.1328]; M. Chakraborti, U. Chattopadhyay, S. Rao and D. P. Roy, Phys. Rev. D **91**, 035022 (2015) [arXiv:1411.4517]; L. Roszkowski, E. M. Sessolo and A. J. Williams, JHEP **1502**, 014 (2015) [arXiv:1411.5214]; A. Chatterjee, A. Choudhury, A. Datta and B. Mukhopadhyaya, JHEP **1501**, 154 (2015) [arXiv:1411.6467]; G. Belanger, D. Ghosh, R. Godbole and S. Kulkarni, [arXiv:1506.00665].

[34] C. Cheung, L. J. Hall, D. Pinner and J. T. Ruderman, JHEP **1305**, 100 (2013) [arXiv:1211.4873]; P. Huang and C. E. M. Wagner, Phys. Rev. D **90**, no. 1, 015018 (2014) [arXiv:1404.0392 [hep-ph]]; L. Roszkowski, S. Trojanowski and K. TurzyÅĎski, JHEP **1411**, 146 (2014) [arXiv:1406.0012 [hep-ph]]; M. E. C. Catalan, S. Ando, C. Weniger and F. Zandanel, arXiv:1503.00599 [hep-ph].

[35] Muon G-2 Collaboration, Phys. Rev. D73 (2006) 072003 [arXiv:hep-ex/0602035]; B. L. Roberts, Chin. Phys. C34 (2010) 741 [arXiv:1001.2898].

[36] T. Sjostrand, S. Mrenna and P. Skands, JHEP **05** (2006) 026 [arXiv:hep-ph/0603175].

[37] XENON100 Collaboration, E. Aprile *et al.*, Phys. Rev. Lett. 109, 181301 (2012) [arXiv:1207.5988].

[38] D. S. Akerib *et al.* [LUX Collaboration], Phys. Rev. Lett. **112**, 091303 (2014) [arXiv:1310.8214].

[39] R. Abbasi *et al.* [IceCube Collaboration], Phys. Rev. D **85**, 042002 (2012) [arXiv:1112.1840];

[40] M. G. Aartsen *et al.* [IceCube Collaboration], Phys. Rev. Lett. **110**, 131302 (2013) [arXiv:1212.4097].

[41] XENON1T Collaboration, E. Aprile *et al.*, [arXiv:1206.6288].

[42] W. Beenakker *et al.*, Phys. Rev. Lett. **83**, 3780 (1999) [Phys. Rev. Lett. **100**, 029901 (2008)] [arXiv:hep-ph/9906298]; Nucl. Phys. B **515**, 3 (1998) [arXiv:hep-ph/9610490].

[43] ATLAS Collaboration, ATLAS-CONF-2013-035 [https://cds.cern.ch/record/1532426].

[44] ATLAS Collaboration, ATLAS-CONF-2013-049 [https://cds.cern.ch/record/1547565].

[45] F. Jegerlehner and A. Nyffeler, Phys. Rept. 477 (2009) 1-110 [arXiv:0902.3360].

[46] K. Hagiwara, R. Liao, A. D. Martin, D. Nomura and T. Teubner, J. Phys. G G38 (2011) 085003 [arXiv:1105.3149].

[47] A. Nyffeler, Nuovo Cim. C **037**, no. 02, 173 (2014) [arXiv:1312.4804] and references therein.

[48] D. A. Kosower, L. M. Krauss and N. Sakai, Phys. Lett. B **133**, 305 (1983); T. C. Yuan, R. Arnowitt, A. H. Chamseddine and P. Nath, Z. Phys. C **26**, 407 (1984).

[49] J. L. Lopez, D. V. Nanopoulos and X. Wang, Phys. Rev. D **49**, 366 (1994); U. Chattopadhyay and P. Nath, Phys. Rev. D **53**, 1648 (1996) [arXiv:hep-ph/9507386].

[50] T. Moroi, Phys. Rev. D **53**, 6565 (1996) (erratum - Phys. Rev. D **56**, 4424 (1997)) [arXiv:hep-ph/9512396]; S. Heinemeyer, D. Stockinger and G. Weiglein, Nucl. Phys. B **690** (2004) 62 [arXiv:hep-ph/0312264] ; G. -C. Cho, K. Hagiwara, Y. Matsumoto and D. Nomura, JHEP **11** (2011) 068 [arXiv:1104.1769].

[51] M. Endo, K. Hamaguchi, S. Iwamoto, T. Yoshinaga, JHEP **01** (2014) 123 [arXiv:1303.4256].

[52] S. Akula, P. Nath and G. Peim, Phys. Lett. B **717** (2012) 188-192 [arXiv:1207.1839]; H. Baer *et al.*, Phys. Rev. D **87**, 035017 (2013) [arXiv:1210.3019].

[53] S. Mohanty, S. Rao and D. P. Roy, JHEP **09** (2013) 027 [arXiv:1303.5830]; S. Akula and P. Nath, Phys. Rev. D **87** (2013) 115022 [arXiv:1304.5526]; N. Okada, S. Raza and Q. Shafi, arXiv:1307.0461; J. Chakrabortty, S. Mohanty and S. Rao, JHEP **02** (2014) 074 [arXiv:1310.3620]. S. P. Das, M. Guchait and D. P. Roy, Phys. Rev. D **90**, no. 5, 055011 (2014) [arXiv:1406.6925]; S. Iwamoto, T. T. Yanagida and N. Yokozaki, [arXiv:1407.4226]; K. Kowalska, L. Roszkowski, E. M. Sessolo and A. J. Williams, JHEP **1506**, 020 (2015) [arXiv:1503.08219]; J. Chakrabortty, A. Choudhury and S. Mondal, [arXiv:1503.08703].

[54] U. Chattopadhyay and P. Nath, Phys. Rev. Lett. **86** (2001) 5854 [arXiv:hep-ph/0102157]; U. Chattopadhyay and P. Nath, Phys. Rev. D **66** (2002) 093001 [arXiv:hep-ph/0208012].

[55] A. Djouadi, J. L. Kneur and G. Moultaka, Comp. Phys. Comm. **176**, 426 (2007) [arXiv:hep-ph/0211331].

[56] A. Djouadi, M. M. Muhlleitner and M. Spira, Acta Phys. Polon. B **38**, 635 (2007) [arXiv:hep-ph/0609292].

[57] G. Belanger, F. Boudjema, A. Pukhov and A. Semenov, Comput. Phys. Commun. **185** (2014) 960 [arXiv:1305.0237].

[58] G. Degrassi, S. Heinemeyer, W. Hollik, P. Slavich and G. Weiglein, Eur. Phys. J. C **28**, 133 (2003) [arxiv:hep-ph/0212020]; B. C. Allanach, A. Djouadi, J. L. Kneur, W. Porod and P. Slavich, JHEP **09**, 044 (2004) [arxiv:hep-ph/0406166]; S. P. Martin, Phys. Rev. D **75**, 055005 (2007) [arxiv:hep-ph/0701051]; R. V. Harlander, P. Kant, L. Mihaila and M. Steinhauser, Phys. Rev. Lett.(100,191602,2008) [arXiv:0803.0672], Erratum: Phys. Rev. Lett.(101,039901,2008); S. Heinemeyer, O. Stal and G. Weiglein, Phys. Lett. B **710**, 201 (2012) [arXiv:1112.3026]; A. Arbey, M. Battaglia, A. Djouadi and F. Mahmoudi, [arXiv:1207.1348].

[59] N. Bhattacharyya and A. Datta, Phys. Rev. D **80**, 055016 (2009) [arXiv:0906.1460].

[60] V. Khachatryan *et al.* [CMS Collaboration], Eur. Phys. J. C **75**, no. 5, 235 (2015) [arXiv:1408.3583]; G. Aad *et al.* [ATLAS Collaboration], Eur. Phys. J. C **75**, no. 7, 299 (2015) [arXiv:1502.01518].

[61] D. Barducci, A. Belyaev, A. K. M. Bharucha, W. Porod and V. Sanz, JHEP **1507**, 066 (2015) [arXiv:1504.02472].

[62] U. Chattopadhyay and D. P. Roy, Phys. Rev. D **68**, 033010 (2003) [hep-ph/0304108]; N. Arkani-Hamed, A. Delgado and G. F. Giudice, Nucl. Phys. B **741**, 108 (2006) [hep-ph/0601041].

[63] The LEP SUSY Working Group, http://lepsusy.web.cern.ch/lepsusy/.

[64] J. R. Ellis, J. S. Hagelin, D. V. Nanopoulos, K. A. Olive and M. Srednicki, Nucl. Phys. B **238**, 453 (1984); K. Griest, Phys. Rev. D **38**, 2357 (1988) [Phys. Rev. D **39**, 3802 (1989)]; K. Griest, Phys. Rev. Lett. **61**, 666 (1988); M. Drees and M. M. Nojiri, Phys. Rev. D **47**, 376 (1993) [hep-ph/9207234].

[65] M. Drees and M. Nojiri, Phys. Rev. D **48**, 3483 (1993) [hep-ph/9307208].

[66] J. Hisano, K. Nakayama and M. Yamanaka, Phys. Lett. B **684**, 246 (2010) [arXiv:0912.4701 [hep-ph]].

[67] A. Gould, Astrophys. J. **321**, 560 (1987); A. Gould, Astrophys. J. **321**, 571 (1987).

[68] K. Griest and D. Seckel, Nucl. Phys. B **283**, 681 (1987) [Erratum-ibid. B **296**, 1034 (1988)].

[69] G. Wikstrom and J. Edsjo, JCAP **0904**, 009 (2009) [arXiv:0903.2986 [astro-ph.CO]].

[70] P. Agrawal, Z. Chacko, C. Kilic and R. K. Mishra, arXiv:1003.5905 [hep-ph].

[71] A. Ibarra, M. Totzauer and S. Wild, JCAP **1404**, 012 (2014) [arXiv:1402.4375 [hep-ph]].

[72] P. Scott *et al.* [IceCube Collaboration], JCAP **1211** (2012) 057 [arXiv:1207.0810 [hep-ph]].

[73] A. Ibarra, M. Totzauer and S. Wild, JCAP **1312** (2013) 043 [arXiv:1311.1418 [hep-ph]].

[74] R. Catena, arXiv:1503.04109 [hep-ph].

[75] ATLAS Collaboration, ATLAS-CONF-2013-047 [http://cds.cern.ch/record/1547563].

[76] ATLAS Collaboration, ATLAS-CONF-2013-062 [http://cds.cern.ch/record/1557779].

[77] ATLAS Collaboration, ATLAS-CONF-2013-007 [https://cds.cern.ch/record/1522430].

[78] ATLAS Collaboration, ATLAS-CONF-2013-061 [http://cds.cern.ch/record/1557778].

[79] A. Datta, A. Datta and S. Raychaudhuri, Phys. Lett. B **349**, 113 (1995) [arXiv:hep-ph/9411435]; A. Datta, A. Datta and S. Raychaudhuri, Eur. Phys. J. C **1**, 375 (1998) [arXiv:hep-ph/9605432].

[80] C. H. Chen, M. Drees and J. F. Gunion, Phys. Rev. Lett. **76**, 2002 (1996) [arXiv:hep-ph/9512230].

[81] ATLAS Collaboration, ATLAS-CONF-2012-043 [https://cds.cern.ch/record/1435197].

[82] P. M. Nadolsky *et al*, Phys. Rev. D **78**, 013004 (2008) [arXiv:0802.0007].